PLOS PATHOGENS

RESEARCH ARTICLE

Intestinal Serum amyloid A suppresses systemic neutrophil activation and bactericidal activity in response to microbiota colonization

Caitlin C. Murdoch[1], Scott T. Espenschied[1], Molly A. Matty[1], Olaf Mueller[1], David M. Tobin[1,2,3], John F. Rawls[1,3]*

1 Department of Molecular Genetics and Microbiology, Duke University School of Medicine, Durham, North Carolina, United States of America, **2** Department of Immunology, Duke University School of Medicine, Durham, North Carolina, United States of America, **3** Department of Medicine, Duke University School of Medicine, Durham, North Carolina, United States of America

* john.rawls@duke.edu

Citation: Murdoch CC, Espenschied ST, Matty MA, Mueller O, Tobin DM, Rawls JF (2019) Intestinal Serum amyloid A suppresses systemic neutrophil activation and bactericidal activity in response to microbiota colonization. PLoS Pathog 15(3): e1007381. https://doi.org/10.1371/journal.ppat.1007381

Editor: Denise M. Monack, Stanford University School of Medicine, UNITED STATES

Received: October 2, 2018

Accepted: January 9, 2019

Published: March 7, 2019

Data Availability Statement: All data are available from Dryad (doi:10.5061/dryad.174667c). 16S rRNA sequencing data have been deposited in the NCBI SRA (PRJNA512204).

Funding: This work was supported by NIH grant P01-DK094779 to JFR; AI130236 to DMT; and NSF grant DGE-1644868 to CCM. The Zeiss Z.1 Lightsheet microscope was supported by NIH S10 1S10OD020010-1A1. The funders had no role in

Abstract

The intestinal microbiota influences the development and function of myeloid lineages such as neutrophils, but the underlying molecular mechanisms are unresolved. Using gnotobiotic zebrafish, we identified the immune effector Serum amyloid A (Saa) as one of the most highly induced transcripts in digestive tissues following microbiota colonization. Saa is a conserved secreted protein produced in the intestine and liver with described effects on neutrophils *in vitro*, however its *in vivo* functions remain poorly defined. We engineered *saa* mutant zebrafish to test requirements for Saa on innate immunity *in vivo*. Zebrafish mutant for *saa* displayed impaired neutrophil responses to wounding but augmented clearance of pathogenic bacteria. At baseline, *saa* mutants exhibited moderate neutrophilia and altered neutrophil tissue distribution. Molecular and functional analyses of isolated neutrophils revealed that Saa suppresses expression of pro-inflammatory markers and bactericidal activity. Saa's effects on neutrophils depended on microbiota colonization, suggesting this protein mediates the microbiota's effects on host innate immunity. To test tissue-specific roles of Saa on neutrophil function, we over-expressed *saa* in the intestine or liver and found that sufficient to partially complement neutrophil phenotypes observed in *saa* mutants. These results indicate Saa produced by the intestine in response to microbiota serves as a systemic signal to neutrophils to restrict aberrant activation, decreasing inflammatory tone and bacterial killing potential while simultaneously enhancing their ability to migrate to wounds.

Author summary

The intestine is colonized by complex microbial communities called the microbiota, which impacts diverse aspects of host physiology including development and function of the innate immune system. Neutrophils are phagocytic innate immune cells essential for

study design, data collection and analysis, decision to publish, or preparation of the manuscript.

Competing interests: The authors have declared that no competing interests exist.

host defense against infection. Neutrophil activity is strongly impacted by the microbiota but underlying mechanisms remain poorly defined. Here we show the evolutionarily-conserved secreted host protein Serum amyloid A (Saa) mediates microbiota-dependent effects on systemic neutrophil function. Saa is produced by the intestine and liver in response to the microbiota, but its *in vivo* functions have remained elusive. Using zebrafish, we demonstrate that Saa promotes neutrophil recruitment to peripheral injury yet restricts clearance of pathogenic bacterial infection. Analysis of isolated neutrophils revealed Saa reduces bactericidal activity and expression of pro-inflammatory genes in a microbiota-dependent manner. Transgenic expression of *saa* in the intestine and liver of *saa* mutants was sufficient to rescue mutant phenotypes, and intestinally-derived *saa* also alleviated defects in neutrophil recruitment to peripheral injury in germ-free zebrafish. Collectively, these data establish that Saa induced by the microbiota in the intestine signals systemically to neutrophils, tuning the extent to which they may be activated by other microbes or respond to injury.

Introduction

The vertebrate intestine is densely colonized with complex communities of micro-organisms, collectively referred to as the intestinal microbiota. Studies using gnotobiotic animals have demonstrated that microbiota colonization is required for the normal development of an innate immune system capable of mounting appropriate responses to diverse challenges such as infection and injury [1]. Despite being spatially confined to the intestinal lumen by physical and chemical barriers such as the intestinal epithelium and mucus, the microbiota influences both local and systemic host immune development and function [2, 3]. However, the specific molecular mechanisms by which the microbiota impacts local and systemic host immune responses remain poorly defined.

Intestinal epithelial cells (IECs) serve as the primary host interface with the intestinal microbiota and secrete a myriad of factors following microbial colonization [4]. We and others have hypothesized that these microbiota-induced IEC products may mediate the microbiota's influences on the host immune system [5, 6]. Previous studies have identified a secreted host factor, Serum amyloid A (Saa), that is potently up-regulated in the intestine following microbial colonization in zebrafish and mice [7–11]. SAA is highly conserved amongst vertebrates, existing as a single gene in fishes and birds and as a multi-gene family in mammals [12, 13]. While basal SAA production is stimulated by the microbiota, SAA production is also markedly augmented following acute injury and infection as a part of the acute phase response, whereby circulating levels can reach 1 mg/mL [13–15]. Moreover, SAA is elevated in chronic pathological conditions where both local and circulating concentrations are positively correlated with inflammation. Accordingly, SAA is an established biomarker for chronic inflammatory diseases such as diabetes, atherosclerosis, and inflammatory bowel disease (IBD) [16–20]. Taken together, SAA's high degree of evolutionary conservation coupled with its strong induction following inflammatory stimuli suggests important roles for SAA in health and disease.

Previous studies have reported both pro- and anti-inflammatory effects of SAA on host immune responses. The vast majority of these studies have been conducted *in vitro* using recombinant human SAA (rhSAA), which has been shown to directly influence granulocytes, including monocytes and neutrophils, promoting the production of inflammatory cytokines, reactive oxygen species (ROS), and directing motility [21–25]. Recent reports

have also shown that mammalian SAAs can bind retinol and mediate host responses during infection [8]. Moreover, induction of SAA in the intestine following colonization with specific microorganisms such as segmented filamentous bacteria (SFB) can shape local adaptive immune cell development by promoting Th17 differentiation [26, 27]. However, a fuller assessment of SAA's *in vivo* functional roles has remained elusive due to the existence of multiple SAA gene paralogs in mammals (3 in humans, 4 in mice) and the use of cell-culture based assays performed with rhSAA that behaves dissimilarly to endogenous SAA protein [28, 29].

The existence of a single SAA ortholog in fishes provides interesting opportunities to define SAA's *in vivo* functional roles. We previously demonstrated that partial (~30%) knockdown of *saa* transcript in zebrafish influenced tissue-specific neutrophil behaviors *in vivo*, leading us to hypothesize that Saa regulates neutrophil activity in homeostasis [12]. However, Saa's influence on systemic neutrophil function in homeostasis and in the relevant contexts of injury and infection remained unresolved. Neutrophils are professional phagocytic myeloid cells that play critical roles in host defense against pathogens. The most abundant immune cell in circulation and the first to be recruited to sites of injury, neutrophils eliminate microbial invaders and debris through a variety of mechanisms including phagocytosis, generation of ROS, and secretion of anti-microbial peptides [30, 31]. Neutrophils are conditioned by host and microbially derived signals, including pathogen associated molecular patterns (PAMPs) and damage associated molecular patterns (DAMPs), allowing for proper responses to inflammatory stimuli [32, 33]. Previous studies have shown that microbial colonization of the intestine promotes neutrophil differentiation, activation, and response to peripheral injury [10, 12, 34–39]. However the signaling molecules that mediate these interactions *in vivo* remain largely unknown.

Here, using zebrafish, we demonstrate that Saa is a host factor that signals microbial status in the intestine to extra-intestinal populations of immune cells and directs their responses to inflammatory stimuli. Zebrafish share highly conserved hematopoietic programs with other vertebrates, including specification of myeloid lineages, which can be coupled with optical transparency and genetic tractability to allow for high resolution *in vivo* imaging of innate immune processes [40, 41]. Moreover, the zebrafish genome encodes a single *saa* ortholog, allowing us to generate the first-ever *saa* null vertebrate model. By comparing wild-type (WT) zebrafish to those that lack *saa* or express it only in intestinal epithelial cells or hepatocytes, we reveal Saa's impact on systemic neutrophil activity in homeostasis and following bacterial infection and wounding. Using tissue specific rescue, we demonstrate that liver- and intestinally-derived Saa can shape systemic neutrophil function and intestinal Saa can even restore neutrophil defects observed in germ-free zebrafish.

Results

Saa promotes neutrophil migration during injury and homeostasis

To investigate Saa's effects on neutrophil function *in vivo*, we first generated *saa* mutant zebrafish, identifying three independent deletion alleles all resulting in frameshift mutations within *saa* exon 2 (S1A–S1C Fig). The largest *saa* deletion allele (22 bp, designated *rdu60*, homozygous mutants hereafter referred to as $saa^{-/-}$) resulted in 90% reduced *saa* mRNA (S1D–S1F Fig). $saa^{-/-}$ zebrafish survived to adulthood and exhibited no gross developmental abnormalities (S1H–S1L Fig). We performed caudal fin amputations on WT and $saa^{-/-}$ *Tg(lyz:EGFP)* larvae and quantified neutrophil recruitment to the wound margin, observing fewer neutrophils at 6 hours post-wounding in $saa^{-/-}$ larvae (Fig 1A and 1B, S1N Fig). Further, *in vivo* imaging revealed that neutrophils in the vicinity of the wound moved with reduced mean speed in *saa*

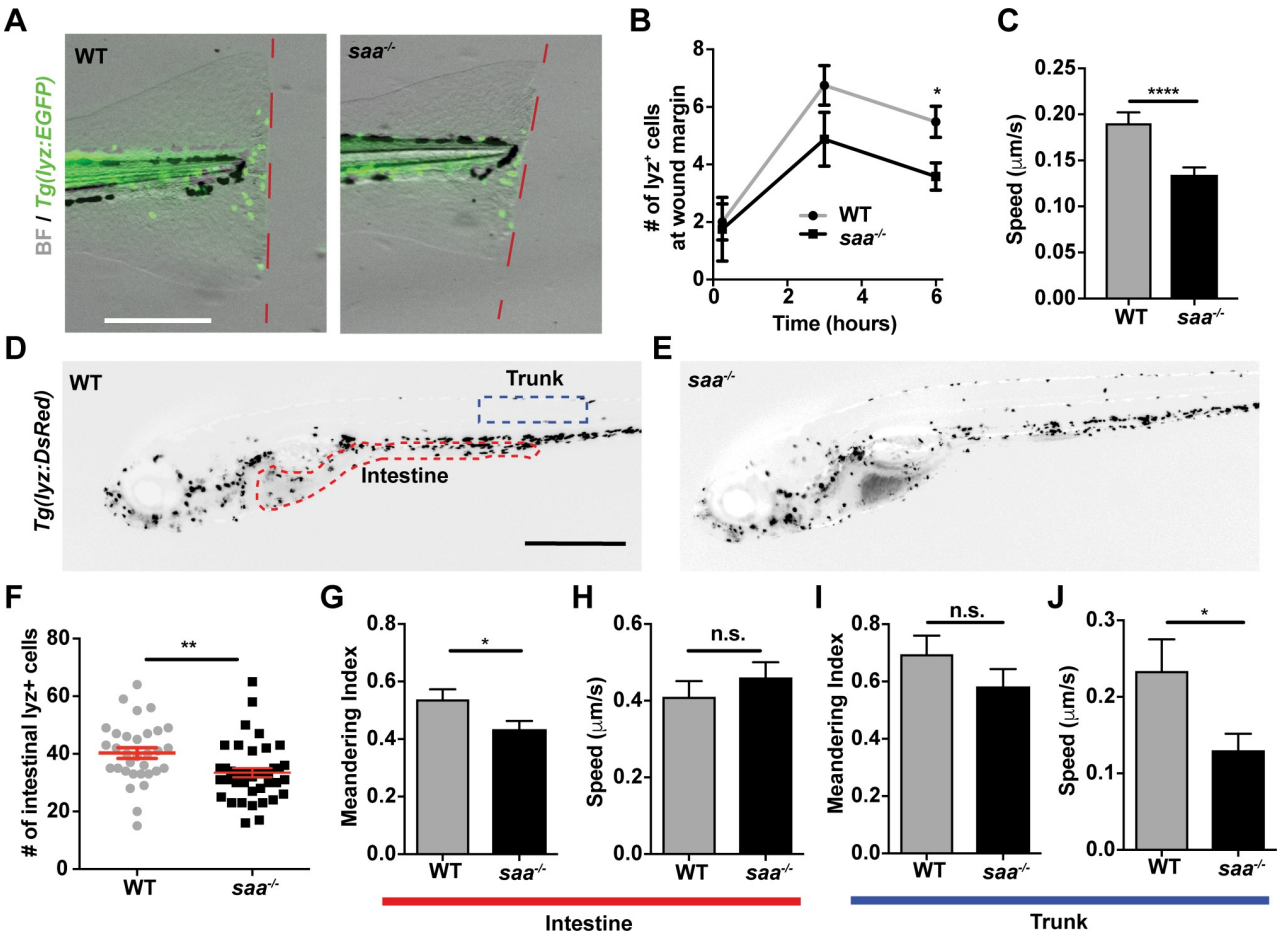

Fig 1. Saa mediates neutrophil behavior *in vivo*. **(A-B)** Imaging and quantification of lyz:EGFP^{+} neutrophils recruited to tail wound margin over 6 hours following caudal fin amputation (dashed red line indicates wound margin; scale bar = 250 μm) (n ≥ 24 larvae / genotype at 6 hour time point). **(C)** Measurement of lyz:DsRed^{+} neutrophil speed from time-lapse imaging in caudal fin tissue over 6 hour period following amputation (n = 4 larvae / genotype, 87–112 cells tracked / genotype). **(D-E)** Representative images of 6 dpf *Tg(lyz:DsRed)* WT and *saa*$^{-/-}$ larvae (scale bar = 500 μm). **(F)** Enumeration of intestine-associated lyz:EGFP^{+} cells in 6 dpf larvae (n = 32–40 larvae / genotype). **(G-J)** Quantitative analysis of lyz:EGFP^{+} neutrophil behavior from time-lapse imaging of distinct anatomical compartments (intestine and trunk, ROIs in panel D) in 6 dpf larval zebrafish (6 larvae / genotype, ≥ 23 cells analyzed / genotype / tissue). Data analyzed by *t*-test. For panel B, statistical comparisons were performed within each time point. Data are presented as mean ± SEM. * $p < 0.05$, ** $p < 0.01$, *** $p < 0.001$, **** $p < 0.0001$.

https://doi.org/10.1371/journal.ppat.1007381.g001

mutant larvae (Fig 1C). Importantly, *saa* mRNA was not upregulated at 6 hours post amputation in WT larvae (S1M Fig), demonstrating acute *saa* induction did not affect neutrophil activity. Thus, Saa is required for neutrophil mobilization to sites of injury independent of systemic induction.

Given that Saa affects neutrophil responses to injury, we tested if Saa regulates basal neutrophil behavior. Analysis of neutrophils in homeostasis revealed Saa promoted neutrophil speed in the trunk and linear migration in the intestine (Fig 1G–1J), consistent with our prior *saa* morpholino knockdown data [12]. Considering *saa* is expressed in IECs [10], we reasoned that Saa may promote neutrophil recruitment to the intestine. Indeed, we observed fewer intestine-associated neutrophils in *saa*$^{-/-}$ larvae (Fig 1D–1F). These data demonstrate that Saa promotes neutrophil recruitment to distinct tissues such as the intestine during homeostasis as well as to peripheral tissues following injury.

Saa restricts systemic neutrophil abundance and bactericidal activity

Given that *saa* loss is associated with impaired neutrophil recruitment to wounds and healthy tissues, we asked whether systemic neutrophil abundance is altered in *saa* mutants. We enumerated systemic neutrophils by flow cytometry (Fig 2A, S2 Fig) and consistently observed elevated neutrophil abundance in $saa^{-/-}$ larvae. This was corroborated by increased expression of the granulocyte marker genes *lysozyme C (lyz)*, *l-plastin (lcp)*, and the granulopoietic cytokine *colony stimulating factor 3a* (*csf3a*, also known as *gcsf1a*) in 6 days post fertilization (dpf) whole larvae (Fig 2D–2F). Morphological classification of lyz^{+} neutrophils into sub-populations from cytospin preparations (adapted from [42]) revealed an over-representation of immature lyz^{+} neutrophils in *saa* deficient animals compared to WT controls (Fig 2B and 2C). Together, these data demonstrate a novel role for Saa regulating neutrophil maturation *in vivo*.

Exposure to PAMPs or inflammatory host molecules can elicit defined neutrophil transcriptional responses, reflecting their activation state [43–47]. Gene expression analysis of FACS-isolated neutrophils revealed elevated expression of genes encoding pro-inflammatory cytokines (*tnfa*, *il1b*), antimicrobial peptides (*pglyrp2*, *pglyrp5*), and regulators of ROS production (*mpx*, *ncf1*) in $saa^{-/-}$ larvae (Fig 3A). These transcriptional differences suggest Saa restricts basal neutrophil activation. As neutrophils primarily function to clear microbial infections [48, 49], we co-cultured neutrophils isolated from adult zebrafish kidneys with non-pathogenic *Escherichia coli* then assessed bacterial viability. Isolated neutrophils from both WT and $saa^{-/-}$ fish were viable *ex vivo* and exhibited morphological responses to bacteria (e.g., extending cytosolic projections; Fig 3B, S3A–S3E and S3J Fig). Co-culture with *E. coli* induced *il1b* mRNA in WT neutrophils, demonstrating zebrafish neutrophils respond transcriptionally to bacteria *ex vivo* (Fig 3C). Moreover, *il1b* transcript levels were significantly increased in unstimulated *saa* mutant adult kidney neutrophils compared to WT, consistent with our observations from larval neutrophils (Fig 3A and 3C). However, following co-culture with *E. coli*, *il1b* in WT neutrophils reached similar levels measured in $saa^{-/-}$ neutrophils (Fig 3C).

To assess neutrophil bactericidal activity, we enumerated CFUs following 4 hours of co-culture and found $saa^{-/-}$ neutrophils killed significantly more bacteria than WT neutrophils (Fig 3D). To interrogate possible mechanisms of bacterial clearance, we labeled neutrophils with CellROX *ex vivo* and measured levels of intracellular ROS by confocal microscopy (S3F and S3G Fig). Bacterial exposure resulted in decreased ROS in both WT and $saa^{-/-}$ neutrophils, indicating bacteria stimulated neutrophil degranulation (Fig 3E). Interestingly, neutrophils from *saa* mutant animals had elevated levels of ROS relative to WT controls both at baseline and after bacterial stimulation (Fig 3E), which is consistent with their augmented bacterial killing activity (Fig 3D). Collectively, these data indicate neutrophils from *saa* mutants are aberrantly activated as evidenced by elevated pro-inflammatory mRNA expression, augmented bactericidal activity, and elevated ROS production, and suggest Saa restricts systemic neutrophil inflammatory tone *in vivo*.

Intestinally-derived Saa alters neutrophil distribution and activity

Since *saa* is highly expressed in the larval zebrafish intestine and liver following microbiota colonization [10], we reasoned that Saa produced by specific tissues might differentially affect systemic neutrophil conditioning. Saa produced by the liver enters circulation and has systemic affects [50], however the distal influences of intestinally-derived *saa* remained unresolved. We generated a transgenic line to drive expression of zebrafish *saa* in hepatocytes using a 2.8 kb promoter fragment from the zebrafish *fabp10a* gene [*Tg(-2.8fabp10a:saa);cmlc2:EGFP*^{rdu66}, hereafter referred to as *Tg(fabp10a:saa)*] [51–54]. We crossed this transgene into

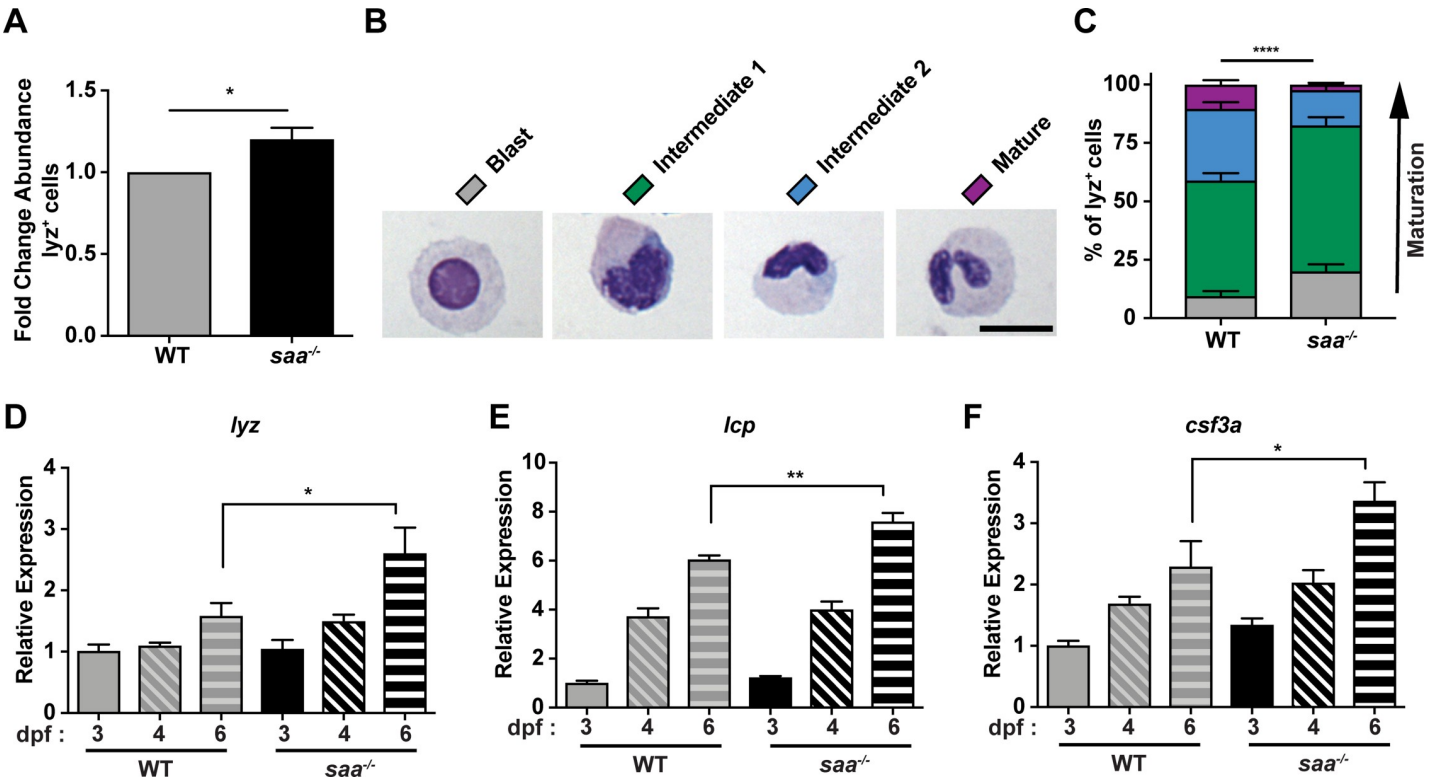

Fig 2. Saa regulates neutrophil abundance and maturation. **(A)** Flow cytometry analysis of lyz:EGFP^{+} neutrophil abundance from whole 6 dpf WT and *saa* mutant zebrafish larvae (results are combined from 3 independent experiments, ≥ 4 replicates / genotype / experiment, 60–90 larvae / replicate). **(B-C)** Morphological analysis of lyz:DsRed^{+} neutrophil cytospins stained with Wright-Giemsa from adult WT and *saa* mutant zebrafish kidneys (5–6 adult zebrafish kidneys / genotype / experiment, 2 independent experiments, n ≥ 199 cells analyzed / genotype / experiment) (scale bar = 10 μm). **(D-F)** qRT-PCR of leukocyte-associated transcripts *lysozyme C (lyz)*, *l-plastin (lcp)*, and *colony-stimulating factor 3a (csf3a)* from 6 dpf whole zebrafish larvae (n = 4 replicates / genotype / timepoint, 25–30 larvae / replicate). Data in panel A analyzed by *t*-test. Data in panel C analyzed by chi-squared test. Data in panels D-F analyzed by one-way ANOVA with Tukey's multiple comparisons test. Data are presented as mean ± SEM. * $p < 0.05$, ** $p < 0.01$, *** $p < 0.001$, **** $p < 0.0001$.

https://doi.org/10.1371/journal.ppat.1007381.g002

the *saa* mutant background and assessed whether hepatic *saa* was sufficient to rescue neutrophil defects observed in *saa* mutant animals.

Despite elevated levels of *saa* transcript in *saa*$^{-/-}$*;Tg(fabp10a:saa)* relative to *saa*$^{-/-}$ mutant larvae (Fig 4A), we still observed reduced intestinal neutrophil recruitment compared to WT controls (Fig 4B). To test the impact of liver-derived *saa* on neutrophil function, we quantified neutrophil recruitment to the wound margin following caudal fin amputation. Neutrophil recruitment at 6 hours post wounding was restored to WT levels in *saa*$^{-/-}$*;Tg(fabp10a:saa)* larvae, demonstrating that hepatic *saa* is sufficient to restore neutrophil response to peripheral injury (Fig 4C). To further investigate the effects of hepatic-derived Saa on neutrophil function, we quantified bactericidal activity of neutrophils from WT, *saa*$^{-/-}$, and *saa*$^{-/-}$*;Tg(fabp10a:saa)* zebrafish. Whereas *E. coli* is cleared quickly by the zebrafish immune system, *Pseudomonas aeruginosa* is capable of establishing systemic infections [55, 56]. Interestingly, transgenic hepatic *saa* was sufficient to restore *P. aeruginosa* killing activity of isolated neutrophils to WT levels in *ex vivo* co-culture (Fig 4D). These data establish that *saa* produced in the liver is capable of influencing a distinct subset of systemic neutrophil functions, promoting their ability to migrate to wounds yet restricting bacterial killing.

Given that the intestine serves as a primary interface between the host and microbiota, and that *saa* is transcriptionally upregulated in the intestine following microbial colonization, we sought to determine if intestinally-derived *saa* could also influence systemic neutrophil

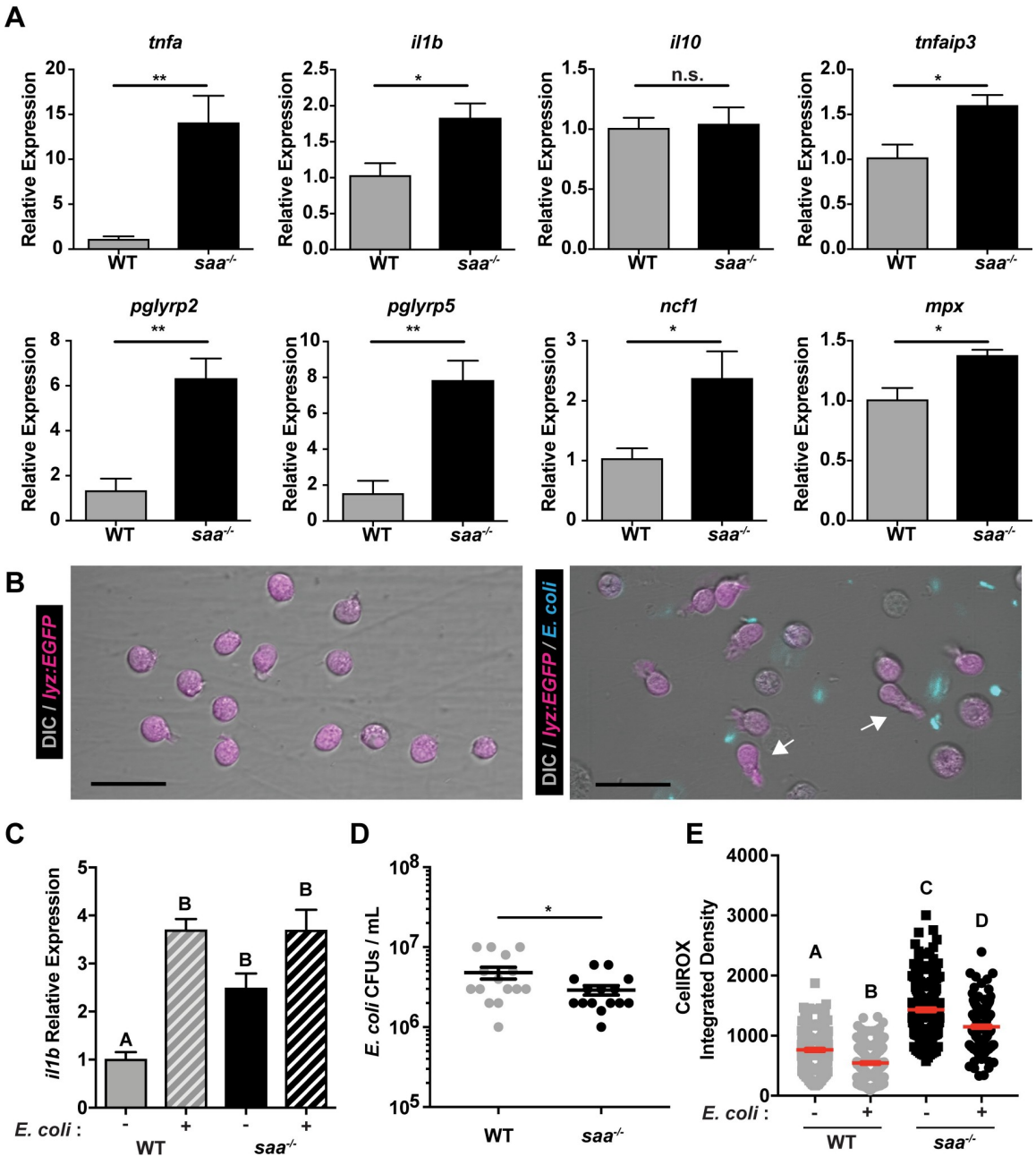

Fig 3. Saa suppresses neutrophil transcriptional activation and bactericidal activity. (A) qRT-PCR of pro-inflammatory mRNAs from sorted neutrophils from 6 dpf WT and *saa* mutant zebrafish larvae (5,000–12,000 lyz:EGFP^{+} cells / replicate, 3–6 replicates / genotype / experiment, 60–90 larvae / replicate). **(B)** Microscopic analysis revealed neutrophils isolated from adult zebrafish kidneys extend protrusions in response to bacterial signals *ex vivo* (white arrows; scale bar = 20 μm). **(C)** *il1b* expression in un-stimulated and *E. coli* exposed lyz:EGFP^{+} neutrophils from WT and *saa* mutant zebrafish following 4 hours *ex vivo* culture (3–5 replicates / genotype / condition). **(D)** CFU quantification of bacterial concentration following 4 hour co-culture of isolated lyz:EGFP^{+} neutrophils from WT and *saa* mutant zebrafish with *E. coli* (MOI 2). **(E)** Quantification of intracellular ROS levels by CellROX fluorescence from neutrophils cultured *ex vivo* with and without *E. coli* (lyz:EGFP^{+} cells isolated from 6 zebrafish adult kidneys / genotype, quantification of ≥ 177 cells / condition). In panels C and E, a one-way ANOVA with Tukey's multiple comparisons test was used. Data in panels A and D were analyzed with a *t*-test. Data are presented as mean ± SEM. * $p < 0.05$, ** $p < 0.01$, *** $p < 0.001$, **** $p < 0.0001$.

https://doi.org/10.1371/journal.ppat.1007381.g003

phenotypes. To do so, we first needed to engineer transgenic zebrafish in which *saa* is expressed specifically in IECs. While several zebrafish promoters have been identified with

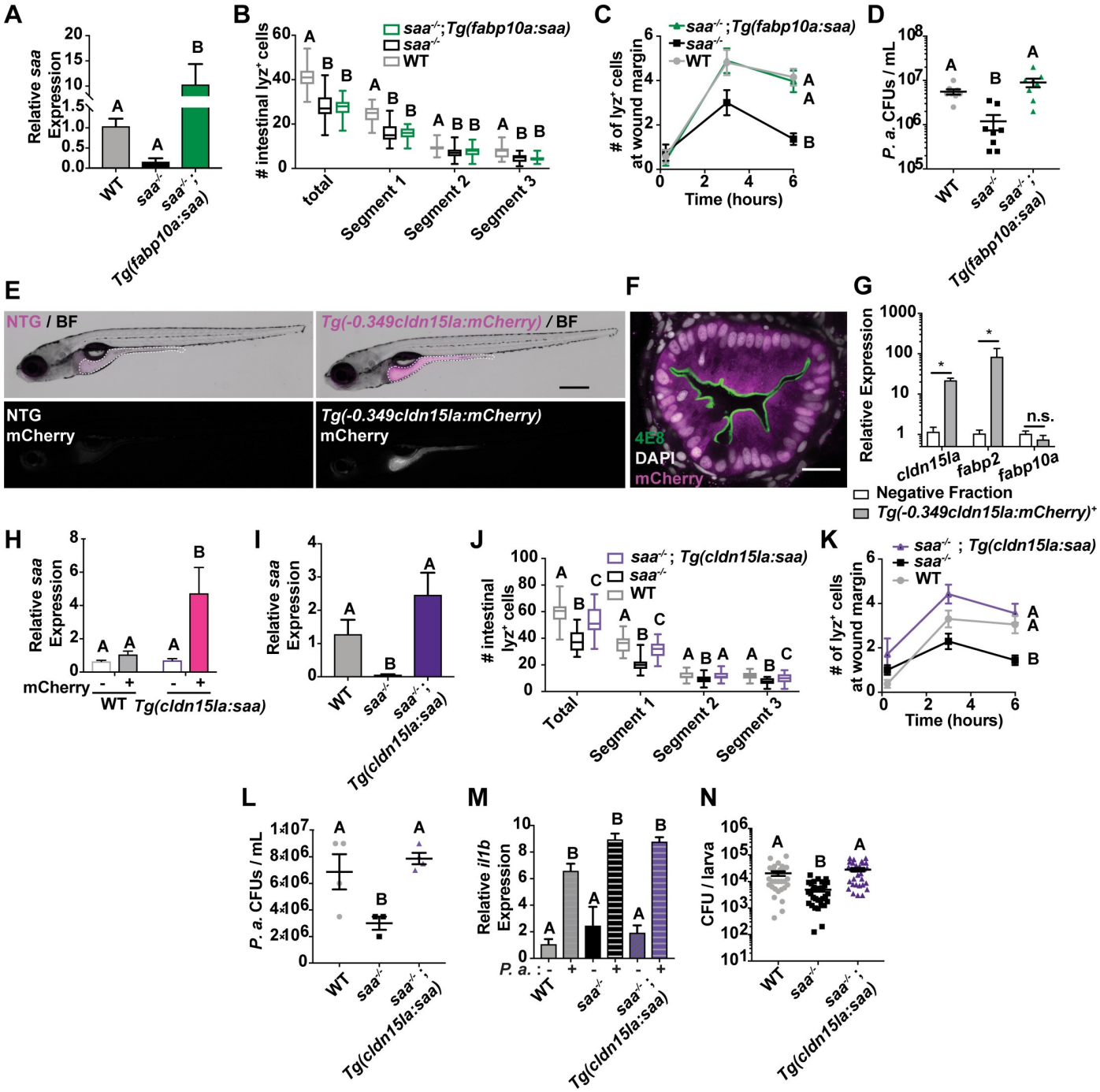

Fig 4. Intestinally-derived Saa regulates systemic neutrophil activity. (A) qRT-PCR of *saa* from whole 6 dpf larvae of the indicated genotypes (n = 4 replicates / genotype, 25–30 larvae / replicate) **(B)** Enumeration of intestine-associated lyz:DsRed^{+} neutrophils along the anterior to posterior axis (segment 1 to segment 3) in 6 dpf larvae (n $\geq$ 25 larvae / genotype). **(C)** lyz:DsRed^{+} neutrophil recruitment to caudal fin wound 6 hours following amputation in 6 dpf zebrafish larvae (n $\geq$ 25 larvae / genotype at 6 hour time point). **(D)** CFU quantification of bacterial concentration following 4 hour co-culture of lyz:DsRed^{+} adult zebrafish neutrophils with *P. aeruginosa* (*P.a.*, MOI 0.2) (8 replicates / genotype). **(E)** Representative stereoscope images of IEC specific mCherry expression in 6 dpf *Tg(-0.349cldn15la:mCherry)^{rdu65}* larvae compared to non-transgenic (NTG) controls. White dashed line indicates the intestine (scale bar = 500 μm). **(F)** Representative confocal micrograph of immunostained transverse section of *Tg(-0.349cldn15la:mCherry)* 6 dpf larvae labeled with the absorptive cell brush border-specific antibody 4E8 (scale bar = 20 μm). **(G,H)** qRT-PCR of *cldn15la*, *fabp2*, and *fabp10a* (G) from sorted *Tg(-0.349cldn15la:mCherry)*$^{+}$ IECs and *saa* (H) from *cldn15la:mCherry*$^{+}$ and negative cells isolated from 6 dpf larvae of indicated genotypes (13,000 –0.349cldn15la:mCherry^{+} or mCherry negative cells / replicate, 4 replicates / genotype, 30 larvae / replicate). **(I)** qRT-PCR of *saa* from 6 dpf larval dissected digestive tissue of the indicated genotypes (n = 4 replicates / genotype, 25–30 larvae / replicate) **(J)** Enumeration of intestine-associated lyz:DsRed^{+} neutrophils in 6 dpf larvae (n = 30 larvae / genotype). **(K)** lyz:DsRed^{+} neutrophil recruitment to caudal fin wound 6

hours following amputation in 6 dpf zebrafish larvae (n ≥ 18 larvae / genotype at 6 hour time point). **(L)** CFU quantification of bacterial concentration following 4 hour co-culture of lyz:DsRed$^+$ adult zebrafish neutrophils with *P. aeruginosa* (*P.a.*, MOI 0.2) (3–6 replicates / genotype). **(M)** *il1b* qRT-PCR from lyz:DsRed$^+$ neutrophils co-cultured with and without *P.a. ex vivo* for 4 hours (n ≥ 2 replicates / condition). **(N)** CFU quantification of *in vivo P.a.* bacterial burden following systemic infection of larval zebrafish at 5 days post infection (dpi) (data from 3 independent experiments, n ≥ 30 larvae / genotype). Data in panels A-D and H-N were analyzed by one-way ANOVA with Tukey's multiple comparisons test. A Mann-Whitney test was applied to panel G. For panels C and K, statistical comparisons were performed amongst samples within the same time point. Data are presented as mean ± SEM. * $p < 0.05$, ** $p < 0.01$, *** $p < 0.001$, **** $p < 0.0001$.

https://doi.org/10.1371/journal.ppat.1007381.g004

intestine-restricted activity, they only drive transgene expression in subsets of IECs (e.g., the *fabp2*/*ifabp* promoter is active in enterocytes in the anterior intestine) [10, 57]. Since zebrafish *cldn15la* is expressed more broadly and specifically in IECs [58, 59], we queried adult zebrafish IEC FAIRE-seq data and identified a 349 bp open chromatin region in the *cldn15la* promoter which contains predicted binding sites for intestine-specific transcription factors including Cdx2 (S4A and S4B Fig) [60]. To confirm intestinal specificity of this *cldn15la* promoter fragment, we used this element to drive expression of *mCherry* [*Tg(-0.349cldn15la:mCherry)*], and observed mCherry fluorescence restricted to IECs (Fig 4E and 4F, S4C–S4F Fig, S5A–S5E Fig) [60, 61]. Gene expression analysis of enterocyte marker *fabp2* and pan-IEC marker *cldn15la* in FACS-isolated mCherry$^+$ and negative cells from *Tg(-0.349cldn15la:mCherry)* larvae revealed strong enrichment in the mCherry$^+$ fraction, further validating the IEC specificity of this promoter (Fig 4G, S4G and S4H Fig).

We next generated *Tg*(*-0.349cldn15la:saa;cmlc2:EGFP*) zebrafish [subsequently denoted *Tg (cldn15la:saa)*], which express zebrafish *saa* in IECs (S6A and S6B Fig). To confirm that *saa* expression was restricted to IECs, we crossed *Tg(-0.349cldn15la:mCherry)* and *Tg(cldn15la:saa)* adults, then sorted mCherry$^+$ IECs and measured levels of *saa* expression in mCherry$^+$ and negative fractions from WT and *Tg(cldn15la:saa)* 6 dpf larvae (S4G and S4H Fig). We observed significantly higher *saa* levels in mCherry$^+$ IECs isolated from *Tg(cldn15la:saa)* larvae compared to WT IECs and both negative fractions (Fig 4H). This data indicates that *saa* expression in *Tg(cldn15la:saa)* larvae is driven specifically in IECs.

We crossed this transgene into the *saa* mutant background, and asked whether IEC-derived Saa could complement *saa*$^{-/-}$ neutrophil defects. As expected, we observed fewer intestine-associated neutrophils in each intestinal segment of *saa*$^{-/-}$ larvae (from anterior to posterior, segments 1–3). Intestinally-derived Saa was sufficient to partially complement this mutant phenotype, with an increased abundance of intestine-associated neutrophils in all segments (Fig 4I and 4J). Thus Saa produced in IECs, unlike hepatic Saa, is sufficient to promote neutrophil recruitment to the intestine, suggesting Saa is a neutrophil chemoattractant *in vivo*. To determine if systemic neutrophil function was altered by intestinally-derived Saa, we performed caudal fin amputations. At 6 hours post amputation, neutrophil recruitment to the wound in *saa*$^{-/-}$*;Tg(cldn15la:saa)* larvae was equivalent to the WT response (Fig 4K), demonstrating intestinally-derived *saa* is sufficient to restore neutrophil mobilization to the caudal fin in otherwise *saa* deficient larvae.

To test the effects of intestinally-derived Saa on neutrophil function, we measured bactericidal activity of neutrophils from WT, *saa*$^{-/-}$, and *saa*$^{-/-}$*;Tg(cldn15la:saa)* zebrafish. We observed reduced survival of both *P. aeruginosa* and *E. coli* following co-culture with *saa*$^{-/-}$ neutrophils vs WT controls. However, neutrophils from *Tg(cldn15la:saa)*$^+$ *saa*$^{-/-}$ zebrafish exhibited comparable bactericidal activity to WT neutrophils (Fig 4L, S6D Fig). Additionally, following *P. aeruginosa* co-culture, neutrophils from WT, *saa* mutant, and *saa*$^{-/-}$*;Tg(cldn15la:saa)* zebrafish exhibited comparable *il1b* transcript induction (Fig 4M), demonstrating that neutrophils from each genotype are responsive to bacterial stimulation *ex vivo*. These findings demonstrate intestinally-derived Saa is sufficient to constrain bactericidal activity of neutrophils.

Considering the profound effects of *saa* levels and source on neutrophil antibacterial function *ex vivo*, we asked if intestinal Saa influenced bacterial clearance *in vivo* using systemic *P. aeruginosa* infection. As neutrophils play an important role in *P. aeruginosa* clearance *in vivo* [62, 63], we postulated that differences in bacterial clearance between WT and *saa* deficient larvae would be largely driven by differences in neutrophil activation and behavior. Larval zebrafish were injected with *P. aeruginosa* via the caudal vein to achieve systemic infection and bacterial burden was assessed from whole zebrafish larvae. Consistent with our *ex vivo* results, we observed enhanced bacterial clearance in *saa*$^{-/-}$ larvae which is restored to WT levels in *saa*$^{-/-}$*;Tg(cldn15la:saa)* larvae (Fig 4N).

Flow cytometry revealed that transgenic intestinal Saa did not significantly alter systemic neutrophil abundance in *saa*$^{-/-}$ larvae whereas liver derived Saa returned neutrophil abundance to WT levels (S7A and S7C Fig). Moreover, qRT-PCR analysis of neutrophils isolated from both *saa*$^{-/-}$*;Tg(cldn15la:saa)* and *saa*$^{-/-}$*;Tg(fabp10a:saa)* larvae revealed persistently elevated expression of pro-inflammatory and anti-microbial effectors (*pglyrp2*, *tnfa*, *il1b*, *ncf1*) (S7B and S7D Fig). Thus, liver and intestinal expression of *saa* was sufficient to rescue only a subset of neutrophil defects observed in *saa* mutant animals. These observations highlight the potential requirement for other tissue sources, presentation, or temporal control of Saa to condition different aspects of systemic neutrophil function. Collectively, these data demonstrate that expression of *saa* in the intestinal epithelium and liver is sufficient to promote neutrophil recruitment to a peripheral wound and to restrict bactericidal activity *in vivo* and *ex vivo*, but is unable to dampen elevated neutrophil pro-inflammatory mRNA profiles observed in *saa* mutant zebrafish. These results further resolve the local and systemic roles for intestinal Saa, promoting neutrophil recruitment to the intestine as well as shaping systemic neutrophil migratory and bacterial killing activity.

Microbiota-induced Saa suppresses neutrophil pro-inflammatory mRNA production and promotes migration to a tail wound

We and others have shown that the intestinal microbiota influences a variety of neutrophil phenotypes both in homeostasis and following injury [12, 36–38]. Since our results indicate that Saa suppresses neutrophil activation (Fig 3A, 3D and 3E) and previous studies have reported Saa has direct bactericidal activity [64–66] we speculated that *saa* deficiency may impact microbiota composition. We used 16S rRNA gene sequencing to compare bacterial communities in the digestive tracts of co-housed *saa*$^{-/-}$ and WT sibling zebrafish at both larval and adult stages. We found that *saa* genotype had no significant effects on gut bacterial community composition as measured by alpha- or beta-diversity metrics at larval (6 dpf) or adult (70 dpf) stages (S2 and S3 Tables). These findings indicate that Saa does not broadly impact gut microbiota composition in zebrafish.

Since *saa* is potently induced following microbial colonization (Fig 5A), we asked if Saa regulates neutrophil activation in response to the microbiota. We isolated neutrophils from 6 dpf gnotobiotic WT and *saa*$^{-/-}$ larvae, and found expression of pro-inflammatory mRNAs was significantly elevated in WT neutrophils from conventionalized (CV) zebrafish vs germ-free (GF) controls, confirming microbiota-derived signals induce neutrophil pro-inflammatory mRNA expression (Fig 5B). Comparison of the same transcripts in neutrophils from *saa*$^{-/-}$ zebrafish reared under CV and GF conditions revealed augmented induction of mRNAs following microbiota colonization. Since neutrophil pro-inflammatory mRNA levels were comparable between WT GF and *saa*$^{-/-}$ GF larvae, we conclude the microbiota potentiates transcriptional activation observed in *saa*$^{-/-}$ larvae (Fig 5B). To assess the impact of the microbiota on neutrophil function in WT and *saa* mutant animals, we measured neutrophil recruitment to

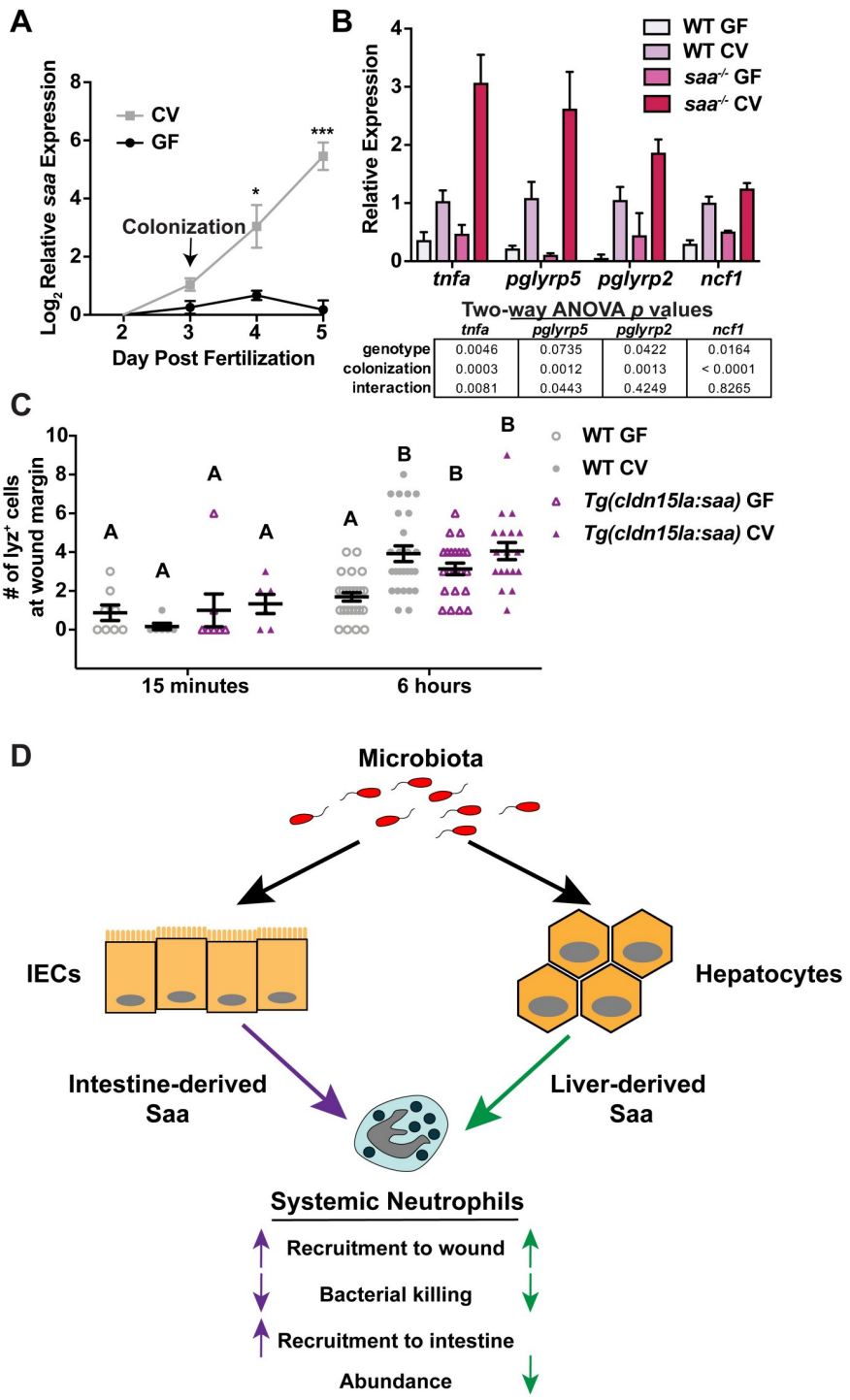

Fig 5. Microbiota-induced Saa conditions neutrophils *in vivo*. **(A)** qRT-PCR of *saa* from gnotobiotic zebrafish larvae following microbiota colonization (CV) at 3 dpf versus germ free (GF) (3 replicates / condition / timepoint, n ≥ 20 larvae / replicate). **(B)** qRT-PCR of neutrophils isolated from 6 dpf gnotobiotic WT and *saa* mutant zebrafish larvae (3 replicates / genotype / condition, n ≥ 27 larvae / replicate). **(C)** lyz:EGFP^{+} neutrophil recruitment to caudal fin wound margin 6 hours after amputation in 6 dpf gnotobiotic WT and *Tg(cldn15la:saa)* sibling zebrafish larvae (n ≥ 18 larvae / genotype / condition at the 6 hour timepoint). **(D)** Working model depicting signals from the microbiota evoking production of intestinal and hepatic Saa leading to shared and distinct effects on systemic neutrophil function. Statistical comparisons of data in panel in A were performed within each time point and analyzed by *t*-test. Data in panel B analyzed by two-way ANOVA with *p* values reported in the table. Data in panel C analyzed

by one-way ANOVA with Tukey's multiple comparisons test. Data are presented as mean ± SEM. * $p < 0.05$, ** $p < 0.01$, *** $p < 0.001$, **** $p < 0.0001$.

https://doi.org/10.1371/journal.ppat.1007381.g005

peripheral tail wound injury in GF larvae. Unlike our previous observations in conventionally reared larvae (Fig 1B), neutrophil recruitment to the fin wound was indistinguishable in GF *saa*$^{-/-}$ and GF WT larvae at 6 hours post wounding (S8A Fig). This indicates that neutrophil recruitment defects only manifest in *saa*$^{-/-}$ mutants when colonized with a microbiota. These data further demonstrate that Saa functions to restrict aberrant activation of neutrophils by the microbiota at homeostasis, thus allowing neutrophils to respond appropriately to injury.

Given that the microbiota induces *saa* expression in the intestine, and GF WT zebrafish larvae have diminished neutrophil responses to wounding compared to conventionalized WT siblings [10], we asked if transgenic *saa* expression in IECs was sufficient to rescue neutrophil deficiencies in GF animals. Consistent with previous findings, we observed reduced neutrophil wound recruitment to caudal fin amputation in GF WT larvae vs CV controls [12]. Transgenic intestinal *saa* expression in GF larvae rescued neutrophil mobilization to the wound margin 6 hours after injury (Fig 5C). These data support a working model wherein Saa produced by IECs in response to the microbiota promotes local recruitment of neutrophils to the intestine while limiting aberrant systemic neutrophil activation by the microbiota, thereby allowing neutrophils to effectively respond to subsequent challenges such as peripheral injury (Fig 5D).

Discussion

Previous reports in mice and zebrafish have demonstrated that the microbiota influences diverse aspects of neutrophil biology, including increased abundance and longevity, enhanced wound recruitment, and elevated bacterial killing [10, 12, 34–36, 38, 39, 67]. However, few studies conclusively identify host or microbial factors that mediate the microbiota's influences on neutrophils. Here we demonstrated that Saa induced following colonization transduces information regarding intestinal microbiota, regulating diverse aspects of neutrophil biology (Fig 5D). In colonized zebrafish at homeostasis, Saa promoted neutrophil maturation and mobilization to the intestine while suppressing systemic neutrophil abundance and pro-inflammatory gene expression. During inflammatory challenge, Saa restricted neutrophil anti-bacterial activity yet promoted neutrophil recruitment to a wound. While *in vitro* studies suggest rhSAA (rhSAA; Peprotech, Rocky Hill, NJ, USA) promotes pro-inflammatory cytokine (TNFα, IL-1β, and IL-8) and ROS production [23, 68–72], the pro-inflammatory effects of rhSAA on granulocytes contrasts with reports using purified endogenous SAA [28, 29]. Thus, our *in vivo* analysis clarifies conflicting reports of Saa's effects on neutrophils.

Our results establish Saa as a major host factor mediating microbial control of neutrophil function. Expression of *saa* is negligible in germ-free zebrafish larvae, but is potently induced following microbial colonization [7, 10]. We therefore reasoned that neutrophil defects in colonized *saa*$^{-/-}$ larvae would phenocopy those exhibited in WT germ-free larvae [10, 12, 73, 74]. In accord, we observed decreases in neutrophil migratory behavior, intestinal association, and wound recruitment in GF WT and colonized *saa*$^{-/-}$ larvae. We demonstrated intestinally-derived Saa was sufficient to partially complement neutrophil deficiencies in *saa*$^{-/-}$ zebrafish and could restore neutrophil wound recruitment in defects GF WT larvae. These results indicate that intestinally-derived Saa conditions neutrophils *in vivo* following microbiota colonization. As we have previously shown that colonization with different bacterial taxa leads to varied levels of *saa* induction [11], this signaling axis may facilitate taxa-specific effects on host innate immune development. Further, it is possible that mammalian SAA paralogs similarly condition neutrophils, as a subset of *Saa* genes are induced in mouse intestinal tissues

following microbial colonization [7–9, 64]. As broad-spectrum antibiotics usage can dramatically impact the microbiota [75–77] and antibiotic treatment results in reduced intestinal *Saa* in mice [78], our model predicts antibiotic treatment could be associated with Saa-mediated aberrations in neutrophil function. We speculate that secondary infections that can occur following antibiotic use [79] could be due in part to concomitant alterations in SAA production.

The mammalian SAA gene family is comprised of both constitutively-expressed and acutely-inducible forms. There are four described paralogs in humans and mice, with much focus placed upon the acute forms which are upregulated following inflammatory stimuli as part of the acute phase response [13]. Following injury or trauma, hepatic production of the canonical acute SAA paralogs, SAA1 and SAA2, is dramatically induced. These secreted proteins enter circulation and associate with high density lipoproteins (HDL) [80], although the functional consequences of this interaction remain unclear. Notably, these acute forms are not only expressed in the liver, as they have also been detected in tissues including the small and large intestine where IECs produce them in response to microbial and inflammatory stimuli [7, 8, 26, 64, 81–83]. In contrast, SAA4 is constitutively expressed in the liver and is not induced by the microbiota or injury [13, 81, 84]. Our previous and present analyses indicate that the single zebrafish *saa* homolog is inducible by microbial stimuli with negligible constitutive expression in germ-free animals, suggesting zebrafish have minimal or no constitutive Saa activity.

Whole animal *Saa1*$^{-/-}$*Saa2*$^{-/-}$ double knockout mice (which still possess *Saa3* –an acute extra-hepatic SAA that is a pseudogene in humans) and whole animal *Saa3*$^{-/-}$ knockout mice are both sensitive to chemically-induced enterocolitis [64, 85], suggesting SAA protects against intestinal inflammation. Moreover, following colonization with segmented filamentous bacteria (SFB), induction of SAA1/2 in mouse small intestinal epithelial cells stimulates expression of effector cytokines (IL-17) in T helper cells and promotes Th17 cell expansion and mucosal defense [26, 27, 86]. Our data indicate that IEC-derived Saa is important for neutrophil recruitment to the larval zebrafish intestine, which may play an important homeostatic role in host defense, mitigating breaches in barrier by commensal or pathogenic microbes. Mouse and human SAAs have also been described as retinol binding proteins that can bind dietary vitamin A with important implications in bacterial infections [8]. Furthermore, expression of SAA in IECs and the liver of mice requires dietary vitamin A [8]. We speculate that vitamin A, the microbiota, and perhaps other environmental factors interactively regulate SAA expression and subsequently influence the development and function of the innate immune system.

In this study we uncover tissue specific influences of Saa on both local and systemic neutrophil biology. Although our transgenic lines express *saa* at levels above endogenous *saa* transcript (Fig 4A and 4I, S6A and S6B Fig), we believe these transgenic levels are still within the physiologic range as circulating levels of Saa protein can reach 1 mg/mL [13–15]. Using these tissue specific promoters allowed us to disentangle the contribution of different tissue sources of Saa on host neutrophil responses. Our data indicate that Saa from the intestine and liver can impact neutrophil activities, such as promoting neutrophil recruitment to peripheral injury and suppressing bacterial killing. However, only Saa produced from IECs was sufficient to promote local neutrophil recruitment to the intestine. We speculate that both intestinal and hepatic Saa shape systemic neutrophil responses to injury by entering circulation from their respective origins. In zebrafish, microbiota induction of Saa is NF-κB and Myd88 dependent [10], and microbial factors, including LPS and flagellar function, are sufficient to induce Saa [11, 87]. Future studies aimed at delineating tissue specific induction of Saa by microbial signals are needed to understand how specific bacterial factors promote Saa production. Differential activity of SAA from the intestine versus liver may be due in part to differences in protein complex formation and downstream receptor recognition, as mammalian SAAs are known to

associate with other proteins in HDL particles [88]. Our model suggests that in cases of chronic intestinal inflammation (e.g. inflammatory bowel disease) when SAA is expressed at high levels in the intestine, there may be SAA-mediated impacts on host systemic innate immune function [16–18].

Saa is thought to directly and indirectly influence in epithelial homeostasis in the mammalian intestine through direct bactericidal activity in the intestinal lumen and by shaping host mucosal innate and adaptive immunity [27, 64, 65]. Studies in mice have demonstrated that acute SAAs are expressed in IECs, and can be secreted both into the lumen and basolaterally, potentially aiding in the clearance of pathogenic bacteria [8, 64, 81, 83]. We did not detect significant alterations in intestinal microbiota composition in our *saa* mutant zebrafish when co-housed with WT controls. However, it remains possible that *saa* mutation may impact microbiota composition or density when genotypes are housed separately.

Our discovery that Saa functions in the microbiota-neutrophil axis motivates interest in underlying mechanisms. Neutrophil functions are largely regulated through "priming", whereby microbial products (e.g. LPS, peptidoglycan, and flagellin) and host factors (e.g. TNFα, IL-1β, IL-8, GM-CSF, and ATP) signal to neutrophils, preparing them for response to additional stimuli [32, 89]. Intriguingly, many priming factors are induced in the zebrafish and mammalian intestine by the microbiota (e.g. TNFα, IL-1β, and GM-CSF) [7, 8, 10, 60, 81]. Primed neutrophils exhibit enhanced bacterial killing, altered motility, and transcriptional changes [33]. Once believed to be transcriptionally quiescent, several studies have reported neutrophil transcriptional responses to various priming stimuli *in vitro* [43–45, 47] and *in vivo* [46, 90, 91]. We demonstrate Saa restricts neutrophil pro-inflammatory gene expression and show induction of pro-inflammatory genes in neutrophils from colonized vs GF WT zebrafish, which is augmented in $saa^{-/-}$ larvae. Consistent with our gene expression results, Saa limits primed neutrophil phenotypes of ROS production and bacterial killing *in vivo* and *ex vivo*. We propose Saa is upregulated following microbiota colonization to temper aberrant neutrophil priming by microbial products and production of host inflammatory mediators, thus limiting collateral damage to host tissues [92–94]. Similarly, a recent report using *Saa3* knockout mice demonstrated that SAA3 suppresses bone marrow derived dendritic cell response to LPS [95], mirroring the anti-inflammatory effects of Saa on zebrafish neutrophils demonstrated here. It will be interesting to determine if SAA's pleiotropic effects on diverse cell types are mediated by different receptors, oligomeric state, or binding other molecules such as retinol [96].

Our data reveal that Saa promotes neutrophil maturation in adult zebrafish. A recent study showed that mature neutrophils exhibit increased motility and response to stimuli [97]. While it is possible that altered neutrophil maturation may underlie the phenotypes we observe in *saa* mutants, some maturation-associated phenotypes (e.g. ROS production and bacterial killing) were elevated in neutrophils from $saa^{-/-}$ zebrafish. Thus, Saa may differentially affect neutrophils at different stages of development and maturation.

Collectively, our findings highlight the importance of intestinal and hepatic Saa effecting systemic neutrophil development and function, suppressing their inflammatory tone and increasing mobilization to wounds. More broadly, our findings suggest that the ontogenetic and microbial control of priming factors is important for vertebrate immunological development.

Materials and methods

Ethics statement

Zebrafish studies were approved by the Institutional Animal Care and Use Committees of Duke University Medical Center (protocol number A115-16-05) in accordance with the Public

Health Service Policy on the Human Care and Use of Laboratory Animals under the Unites States of America National Institutes of Health (NIH) Office of Laboratory Animal Welfare (OLAW).

Animal husbandry

All zebrafish lines were maintained on a mixed Tübingen (Tü) / TL background on a 14:10 hour light:dark cycle in a recirculating aquaculture system. From 5 dpf to 14 dpf, larvae were fed Zeigler AP100 <50-micron larval diet (Pentair, LD50-AQ) twice daily and Skretting Gemma Micro 75 (Bio-Oregon, B5676) powder once daily. Beginning at 14 dpf, larvae were fed *Artemia* (Brine Shrimp Direct, BSEACASE) twice daily, supplemented with a daily feed of Skretting Gemma Micro 75. From 28 dpf, the Gemma Micro 75 diet was replaced with Gemma Micro 300 (Bio-Oregon, B2809). At the onset of breeding age or sexual maturity, adult fish were given a 50/50 mix of Skretting Gemma Micro 500 (Bio-Oregon, B1473) and Skretting Gemma Wean 0.5 (Bio-Oregon, B2818) and one feeding of *Artemia* daily.

Larvae were also maintained on a 14:10 hour light:dark cycle in a 28.5˚C incubator, and are of indeterminate sex. Gnotobiotic zebrafish were generated following natural mating and reared as described previously [98] with the following exception: GZM with antibiotics (AB-GZM) was supplemented with 50 μg/ml gentamycin (Sigma, G1264). Conventionally raised zebrafish were maintained at a density of $\leq$ 1 larva / mL, and at 3 dpf groups of 30 larvae were transferred to 10 cm petri dishes containing 20 mL gnotobiotic zebrafish media (GZM), inoculated with 3 mL filtered system water (5μm filter, SLSV025LS, Millipore) and fed autoclaved ZM-000 zebrafish diet (1% w/v stock concentration (in RO H_2O), 0.0025% w/v final concentration, Zebrafish Management Ltd.) [10]. *TgBAC(cldn15la:EGFP)*^{pd1034Tg} (which expresses a Cldn15la-EGFP fusion protein), *Tg(lyz:DsRed)*^{nz50} and *Tg(lyz:GFP)*^{nz117} have been previously characterized [40, 58].

Zebrafish mutagenesis

Targeted deletion of the *saa* gene was performed using CRISPR/Cas9 gene editing targeting the second exon of *saa* as described [7]. Briefly, the guide RNA sequence was designed using the "CRISPR Design Tool" (http://crispr.mit.edu/). Guide RNA oligos (S1 Table, primers P1 and P2) were ligated into pT7-gRNA plasmid (Addgene, 46759), which, following BamHI (New England Biolabs, R0136L) digest, was *in vitro* transcribed using MEGAshortscript T7 kit (ThermoFisher, AM1354) [99]. Cas9 mRNA was generated from XbaI (New England Biolabs, R0145S) digested pT3TS-nls-zCas9-nls plasmid (Addgene, 46757), and *in vitro* transcribed using mMESSAGE mMACHINE T3 kit (ThermoFisher, AM1348) [99]. A cocktail consisting of 150 ng/μL of nls-zCas9-nls and 120 ng/μL of gRNA, 0.05% phenol red, 120 mM KCl, and 20 mM HEPES (pH 7.0) was prepared, and approximately 1–2 nL was injected directly into the cell of one cell stage Tü zebrafish embryos. Mutagenesis was initially screened using Melt Doctor High Resolution Melting Assay (ThermoFisher, 4409535), and identified three independent alleles which were confirmed as deletions by Sanger sequencing of TOPO-cloned PCR products. Subsequent screening of the Δ22 (allele designation *rdu60*) was performed by PCR (primers P3 and P4, S1 Table) and products were resolved on 2% agarose TBE gels. Screening of the Δ2 and Δ5 alleles (allele designations *rdu61* and *rdu62* respectively) was performed by PCR amplification using primers P3 and P4 (S1 Table), followed by purification and Hha1 digest (New England Biolabs, R0139S). All mutant alleles (*rdu60*, *rdu61*, and *rdu62)* result in the loss of a single Hha1 restriction site present in the WT sequence.

Zebrafish transgenesis

For generation of transgenic zebrafish expressing *saa* in intestinal epithelial cells (IECs) or liver hepatocytes, the following strategy was employed utilizing Tol2 mediated transgenesis (https://onlinelibrary.wiley.com/doi/abs/10.1002/dvdy.21343). A 349 bp region of the zebrafish *cldn15la* promoter was PCR amplified from Tü genomic DNA using primers P5 and P6 (S1 Table), digested with FseI and AscI (New England Biolabs, R0588 and R0558), and ligated into the p5E 381 vector that had been linearized with the same enzymes to generate p5E-*0.349cldn15la*. The -2.8 kb *fabp10a* p5E vector was kindly provided by Brian Link. The full-length zebrafish *saa* coding sequence was PCR amplified from Tübingen whole-larvae cDNA using primers P7 and P8 (S1 Table) and subcloned into the plasmid pENTR-AleI using In Fusion (Takara Bio, 638909) to generate pME-*saa*. Both p5E-*0.349cldn15la* and pME-*saa* were verified by PCR and Sanger sequencing. A 4-way Gateway LR reaction was performed using LR Clonase II (ThermoFisher, 12538120) to recombine p5E-*0.349cldn15la* or p5E-*2.8fabp10a*, with pME-*saa*, and p3E-polyA 229 into pDEST 395 (which contains a bicistronic *cmlc2*:*EGFP* reporter), yielding the following constructs: *-0.349cldn15la*:*saa*:*polyA*;*cmlc2*:*EGFP* and *-2.8fabp10a*:*saa*:*polyA;cmlc2*:*EGFP*. These plasmids were co-injected with transposase mRNA into Tü embryos at the single cell stage respectively, as described elsewhere [60]. Injected F_0 larvae were subsequently screened for mosaic EGFP expression in the heart, raised to adulthood, and used to establish stable lines for three independent alleles of *Tg*(*-0.349cldn15la*:*saa*;*cmlc2*:*EGFP*) (*rdu64*, *rdu67*, and *rdu68*) and *Tg(-2.8fabp10a*:*saa;cmlc2*:*EGFP)* (*rdu66*). Experiments were conducted with both larval and adult zebrafish positive for *rdu64*, *rdu67*, *rdu68* and *rdu66* and non-transgenic siblings used as controls.

To confirm IEC specificity of the 349 bp *cldn15la* promoter fragment, we also recombined p5E-0.349*cldn15la*, pME-*mCherry* 386 (cytosolic mCherry), and p3E-polyA with pDEST 394, and injected this construct into single cell Tü embryos. Mosaic F_0 larvae were raised to adulthood, screened for germline transmission, and used to establish stable lines for three independent alleles of *Tg(-0.349cldn15la*:*mCherry*:*polyA)*. All three alleles displayed mCherry expression restricted to the intestine, and allele *rdu65* was maintained for further analysis.

Caudal fin amputation assay

Larval zebrafish were anaesthetized with 0.75 mM Tricaine and mounted in 3% (w/v) methylcellulose (in GZM). Caudal fins were amputated using a surgical scalpel (Surgical Specialties Sharpoint, 72–2201) and fish were revived into 10 cm dishes containing either GZM (for experiments with conventionally reared larvae) or AB-GZM without gentamycin (for experiments with gnotobiotic larvae). At 15 minutes, 3 hours, and 6 hours post wounding, animals were euthanized and fixed in 4% PFA / 1x PBS overnight at 4˚C on an orbital platform. Larvae were subsequently washed with 1x PBS 3–5 times at room temperature. Imaging was performed with a Leica M205 FA equipped with a Leica DFC 365FX camera using either GFP or mCherry filters. Lyz^+ cells were enumerated at the tail wound margin using the Fiji Cell Counter plugin. Fish that were wounded at the notochord or were moribund were excluded from analysis.

In vivo imaging and cell tracking analysis

Larval zebrafish were anaesthetized and mounted in 100 μL 0.75% (w/v in GZM) low melt agarose (Fisher Scientific, BP165-25) with 0.6 mM Tricaine in 96-well clear-bottom black-walled plates (Greiner Bio-One, 655090), and overlaid with 100 μl GZM containing 0.375 mM Tricaine. For homeostatic behavioral analysis, time lapse imaging was performed for 10 or 15 minutes and frames acquired at 30s intervals on a Zeiss Axio Observer with a Photometrics

Evolve EMCCD camera and a 5x objective (NA 0.16, WD 18.5 mm). For live imaging following caudal fin amputation, larvae were mounted as described above and imaged for 6 hours at 2 or 5 minute intervals on an inverted Zeiss Axio Observer Z1 microscope equipped with an Xcite 120Q light source (Lumen Dynamics), an MRm camera (Zeiss), and a 20X objective lens (NA 0.4, WD 7.9 mm). Fish that were wounded at the notochord, moribund, or damaged during mounting were excluded from analysis. Automated cell tracking was performed using the MTrack2 plugin for Fiji. For cell tracking following caudal fin amputation, a region of interest (ROI) was drawn from the posterior end of the notochord to the wound margin. For neutrophil behavior analysis in homeostasis, two distinct ROIs were analyzed. An ROI (396 pixels by 52 pixels, w x h) was drawn over the intestine ending at the cloaca, and another ROI (364 pixels by 152 pixels, w x h) was positioned dorsally to the intestine in the trunk. We subsequently filtered tracking results to include cells that were tracked for $\geq$ 3 consecutive frames. Speed and meandering index were calculated as previously described [12].

Epifluorescence stereomicroscopy

Larval zebrafish from pooled clutches were anaesthetized in 0.75 mM Tricaine and mounted in 3% methylcellulose. Between 15 and 30 fish / genotype were imaged on a Leica M205 FA microscope equipped with a Leica DFC 365FX camera using identical magnification and exposures. Neutrophil recruitment to the intestine was quantified from 8-bit images with Fiji software using the Cell Counter plug in as described previously [12].

For quantifying mCherry fluorescence mean grey values were measured in FIJI. Equal size ROIs were drawn in the liver, trunk, or eye. To quantify intestinal fluorescence, an ROI was drawn around the entire intestine. All mean grey values were normalized by subtracting background signal.

Light sheet microscopy

For *in vivo* light sheet microscopy, 6 dpf zebrafish larvae were anesthetized in 0.75 mM Tricaine in GZM, mixed with 1% LMP Agarose in GZM supplemented with 0.75 mM Tricaine, and drawn up into a glass capillary tube. The agarose was allowed to polymerize for at least 10 minutes prior to imaging. Agarose-embedded larvae were extruded from the capillary into an imaging chamber filled with GZM supplemented with 0.75 mM Tricaine and heated to 28.5˚C. Single Plane Illumination Microscopy (SPIM) was performed with a Zeiss Lightsheet Z.1 Microscope equipped with a 20x aqueous immersion objective (1.0 NA, 2.4 mm WD). Two channel acquisition was performed with frame switching using 488 nm and 561 nm excitation lines, and z-series were acquired with a 7.32 μm interval. Image-processing was performed using 64-bit FIJI.

Fluorescence Activated Cell Sorting (FACS)

For FACS, replicate pools of 60–90 lyz^{+} larvae or 30 *Tg(-0.349cldn15la:mCherry)*$^{+}$ larvae of the indicated genotypes were euthanized with 3 mM Tricaine and washed for 5 minutes with deyolking buffer (55 mM NaCl, 1.8 mM KCl and 1.25 mM $NaHCO_3$). Larvae were transferred to gentleMACS "C" tubes (Miltenyi Biotec, 130-096-334) containing 5 mL Buffer 1 [HBSS supplemented with 5% heat-inactivated fetal bovine serum (HI-FBS, Sigma, F2442) and 10 mM HEPES (Gibco, 15630–080)]. Larvae were dissociated using a combination of enzymatic and mechanical disruption. Following addition of Liberase (Roche, 05 401 119 001, 5 μg/mL final), DNaseI (Sigma, D4513, 2 μg/mL final), Hyaluronidase (Sigma, H3506, 6 U/mL final) and Collagenase XI (Sigma, C7657, 12.5 U/mL final), samples were dissociated using pre-set program C_01 on a gentleMACS dissociator (Miltenyi Biotec, 130-093-235), then incubated at 30˚C on

an orbital platform at 75 RPM for 10 minutes. The disruption-incubation process was repeated 4–6 times, after which 400 μL of ice-cold 120 mM EDTA (in 1x PBS) was added to each sample. Following addition of 10 mL Buffer 2 [HBSS supplemented with 5% HI-FBS, 10 mM HEPES and 2 mM EDTA], samples were filtered through 30 μm cell strainers (Miltenyi Biotec, 130-098-458) into 50 mL conical tubes. Filters were washed with 10 mL Buffer 2, and samples were centrifuged at 1800 rcf for 15 minutes at room temperature. The supernatant was decanted, and cell pellets were resuspended in 500 μl Buffer 2. For CellROX (Invitrogen C10491 or C10444) labeling experiments, cells were then resuspended in 500 μL Buffer 2 and transferred to individual wells of a 24-well plate. CellROX was added to a final concentration of 1 μM, and samples were incubated for 45 minutes in the dark at 28.5˚C on a tilting platform. Samples were transferred to FACS tubes (Falcon, 352052), and DNaseI (5 μg/mL; Sigma, D4513) and 7-AAD (Sigma, A9400, 5 μg/mL) were added. FACS was performed with either Beckman Coulter MoFlo XDP, Beckman Coulter Astrios, Becton Dickinson Diva, or Sony SH800S cell sorters at the Duke Cancer Institute Flow Cytometry Shared Resource. Single-color control samples were used for compensation and gating. Viable neutrophils or IECs were identified as 7-AAD$^-$ lyz$^+$ or 7-AAD$^-$ mCherry$^+$ respectively. Data were analyzed with FloJo v10 (Treestar, CA).

Ex vivo zebrafish neutrophil culture

Kidneys were dissected from adult male and female transgenic lyz$^+$ zebrafish of the indicated genotypes. Fish were of standard length 25.72mm±1.18mm (mean±S.D.). Single cell suspensions were generated by enzymatic treatment of dissected kidneys with DNaseI (2 μg/mL) and Liberase (5 μg/mL final) with gentle agitation on a fixed speed orbital platform (VWR, 82007–202) for 20 minutes at room temperature. Enzymes were deactivated by the addition of EDTA as described above and cell suspensions were filtered through 30 μm filters and either stained with 1 μM CellROX for 1 hour at 28˚C and/or stained with 7-AAD (5 μg/mL) or Propidium Iodide (PI, Sigma, P21493, 5 μg/mL). Viable (7-AAD$^-$ or PI$^-$) lyz$^+$ cells were collected into poly-D-lysine (Sigma, P7280-5MG, 33 μg/mL) coated 96 well black-wall clear-bottom plates (Corning, 3603) containing 100 μl RPMI1640 (Gibco, 11835030) supplemented with 10% HI-FBS at a density of 15,000 cells per well. A total of 6–9 kidneys per genotype were pooled and used to seed 4–6 wells. DsRed-expressing *Escherichia coli* MG1655 (pRZT3, [87]) or GFP-expressing *Pseudomonas aeruginosa* PA01 (pMF230, [62]) were cultured aerobically overnight shaking at 37˚C in LB supplemented with either tetracycline (10 μg/mL) or carbenicillin (100 μg/mL), respectively. Bacteria (100 μL) were subsequently sub-cultured into 5 mL selective LB media and grown at 37˚C with shaking under aerobic conditions to an OD_{600} of 0.7–1, diluted in sterile 1x PBS (Gibco, 14190) to a concentration of 10^4 bacterial / μL (*E. coli*) or 10^3 bacteria / μL (*P. aeruginosa*), and added isolated neutrophils at an MOI of 2 or 0.2 respectively. Neutrophils were co-cultured with bacteria for 2 to 4 hours at 28˚C with gentle agitation in the dark. Serial dilutions of co-culture supernatants were prepared in sterile 1x PBS and plated on selective media. Plates were incubated aerobically at 28˚C for 24 hours and CFUs were enumerated.

For imaging studies, neutrophils were collected as described above with the following modification: cells were collected into poly-D-lysine coated thin-bottom 96 well plates (Greiner, 655090). Neutrophils were imaged on a Zeiss 710 inverted confocal microscope with 10x (NA 0.45) or 63x oil objectives (NA 1.40) with or without addition of bacteria.

To measure neutrophil viability, 96 well black wall clear bottom plates containing 15,000 cells / well were incubated with or without *E. coli* MG1655 (MOI 2, grown as described above) for 3.5 hours. Propidium Iodide (PI) was added to a final concentration of 6 μg/mL to each

well, and plates were incubated for an additional 30 minutes at 28.5˚C before reading fluorescence at 535/620 (Ex/Em, nm) with a BioTek Synergy2 plate reader. As a positive control, lyz^+ cells were incubated with Triton X-100 (20% v/v) for 3 hours, then incubated at 65˚C for 30 minutes prior to PI staining. Data are shown as % of maximum PI signal.

Cytospins and scoring of neutrophil maturation

For morphological assessment, 15,000–30,000 viable lyz^+ cells isolated by FACS from adult dissected kidneys as described above were sorted into 500 μl Buffer 2. Cytospins were performed immediately following collection with a Cytospin 3 (Shandon) by centrifuging cell suspensions for 3 minutes at 800 rcf. Slides were dried overnight at room temperature, fixed with absolute methanol, then stained with Wright Giemsa (Sigma, WG16) according to the manufacturer's instructions. Slides were imaged with a Leica DMRA2 compound microscope with a PL APO 40x air objective (NA 0.85, WD 0.11mm) and Q Imaging Micropublisher Digital color camera. Twenty individual ROIs were imaged per genotype, and cells were classified based on distinct nuclear morphology by a blinded investigator as described [42].

Gene expression analysis

Pools of 20–30 whole larvae, dissected digestive tracts, or carcasses were collected into 1 mL of TRIzol (ThermoFisher, 15596026) and stored at -80˚C. For experiments measuring transcripts from digestive tract versus carcass, dissections were performed as described previously [73] on 6 dpf larvae to remove the digestive tract (including intestine, liver, and pancreas). Digestive tracts were dissected and pooled into TRIzol (15–20 per replicate). The remaining carcasses were collected and pooled into TRIzol. Tissues were homogenized by passing samples 10–15 times through a 27-gauge needle. RNA was isolated following the manufacturer's protocol with the following modification: a second wash with 70% ethanol (prepared in DEPC-treated H_2O) was performed. For gene expression analysis of sorted neutrophils, viable lyz^+ (4000–6000 cells / replicate) cells were collected into 750 μL TRIzol LS (ThermoFisher 10296010). For validation of the *-0.349cldn15la* promoter, 13,000 *Tg(-0.349cldn15la:mCherry)*$^+$ and mCherry negative cells per replicate were collected into 750 μL of TRIzol LS. RNA was isolated using a NORGEN RNA Cleanup and Concentrator Micro-Elute Kit (Norgen Biotek, 61000), and samples eluted in 10 μL from which 8 μL of RNA was treated with DNaseI (New England Biolabs, M0303L). cDNA was synthesized using the iScript kit (Bio-Rad, 1708891). Quantitative PCR was performed in duplicate 25 μl reactions using 2X SYBR Green SuperMix (PerfeCTa, Hi Rox, Quanta Biosciences, 95055) run on an ABI Step One Plus qPCR instrument using gene specific primers (S1 Table). Data were analyzed with the $\Delta\Delta Ct$ method.

In vivo bacterial infections

Pseudomonas aeruginosa PA01 carrying a constitutively expressed GFP plasmid (pMF230) [62] was grown in LB media supplemented with 100 μg/mL carbenicillin overnight shaking at 37˚C. Overnight culture was concentrated to an OD600 of 5 (approximately $2x10^9$ bacteria / mL) then frozen in aliquots. At 1 dpf, larvae were treated with 45 μg/mL 1-phenyl-2-thiourea (PTU) to inhibit melanization. Larvae were infected at 2 dpf by a genotype-blinded investigator. To achieve systemic infection, bacteria were injected into circulation via the caudal vein with borosilicate needles along with a phenol red tracer (3% w/v) as described previously [100], and any larvae that were damaged by injections were excluded from analysis. Approximately 150–300 CFU of *P. aeruginosa* PA01 GFP was injected per larvae. To enumerate CFUs in the inoculum, the injection dose was plated before and after infections on LB agar plates supplemented with 100 μg/mL carbenicllin. Immediately following infection larvae were

screened for even dosing by fluorescence microscopy, and significantly under- or over-infected larvae were excluded from further analysis by an investigator blinded to genotype. To quantify bacterial burden, individual larvae were homogenized in 500 μL sterile 1x PBS using a Tissue-Tearor (BioSpec Products, 985370) at 24 hour intervals, and serial dilutions were plated on selective media (LB agar supplemented with 100 μg/mL carbenicillin). *P. aeruginosa* CFUs were enumerated following aerobic incubation for 24 hours at 28˚C.

Zebrafish immunohistochemistry

For immunostaining, 6 dpf larval zebrafish were fixed in 4% PFA/1x PBS overnight at 4˚C on an orbital platform, then washed 3-5x with 1x PBS the following day. Larvae were mounted in 4% low melt agarose in cryo-molds molds (Tissue-Tek) and 200 μm transverse sections cut using a Leica VT1000S vibratome. Sections were transferred to 24-well plates, washed 3x in 1x PBS at room temperature, and permeabilized with 1x with PBS containing 0.1% (v/v) Triton x-100 (PBS-T) for 30 minutes at RT. Sections were blocked in 5% (v/v) donkey serum in PBS-T for 1 hour at room temperature, then incubated with primary antibodies diluted in blocking buffer overnight at 4˚C with agitation (mouse anti 4E8, Abcam, ab73643, 1:200; mouse anti 2F11, Abcam, ab71286, 1:200; rabbit anti DsRed, Clontech, 632496, 1:200; chicken anti GFP, AVES, GFP-10x0, 1:200). Sections were washed with PBS, then incubated with species-specific secondary antibodies [(ThermoFisher, A10042, A32728, A11039, 1:200) and Hoechst 33258 (ThermoFisher, H3569, 1:1000)] diluted in PBS-T for 2–4 hours at room temperature on a tilting platform. Sections were then washed 3x with 1x PBS then mounted and coverslipped on slides using mounting media containing DAPI (Vector Laboratories, Inc, H-1200). Slides were imaged with a Zeiss LSM 780 upright confocal microscope equipped with a GaAsP array detector using a 63x oil objective (NA 1.4, WD 0.19 mm).

16S rRNA gene sequencing

Adult heterozygous *saa*$^{rdu60/+}$ zebrafish were bred naturally and the resulting embryos were collected into system water and pooled at 0 dpf. Fertilized embryos were sorted at equal densities into autoclaved 3L tanks filled with system water at 1 dpf (50 embryos per 3 liter tank). Zebrafish of both WT and *saa* mutant genotypes were co-housed for the duration of the experiment. Larvae were maintained under static conditions until 6 dpf, at which time water flow and feeding were begun. Dissected digestive tracts and environmental water samples were collected at two time points: 6 dpf and 70 dpf. At 6 dpf zebrafish were sampled prior to first feeding, and fish sampled at 70 dpf were fed using the standard facility diet (as described above in animal husbandry) beginning at 6 dpf. For each timepoint, fish were sampled from a minimum of 5 tanks. For the 6 dpf timepoint DNA was isolated from 14 WT and 15 *saa* mutant intestines. For the 70 dpf timepoint, DNA was isolated from 15 WT and 12 *saa* mutant intestines. For water samples, 50 mL of water was collected from each tank and filtered using 0.2 μm MicroFunnel Filter Units (Pall Corporation, 4803). Filters were removed from filter units with sterile forceps, transferred to Eppendorf tubes and snap frozen in a dry ice/ethanol bath. For intestinal samples, digestive tracts were dissected and flash frozen and either carcasses or fin were reserved for genotyping. Fish samples were genotyped to identify homozygous *saa*$^{+/+}$ and *saa*$^{rdu60/rdu60}$ zebrafish prior to submission for genomic DNA extraction.

The Duke Microbiome Shared Resource (MSR) extracted bacterial DNA from gut and water samples using a MagAttract PowerSoil DNA EP Kit (Qiagen, 27100-4-EP) that allows for the isolation of samples in a 96 well plate format using a Retsch MM400 plate shaker. DNA was extracted from $\geq$12 fish per genotype per time point, and from 5 to 8 different tanks per timepoint to control for tank effects. Sample DNA concentration was assessed using a Qubit

dsDNA HS assay kit (ThermoFisher, Q32854) and a PerkinElmer Victor plate reader. Bacterial community composition in isolated DNA samples was characterized by amplification of the V4 variable region of the 16S rRNA gene by polymerase chain reaction using the forward primer 515 and reverse primer 806 following the Earth Microbiome Project protocol (http://www.earthmicrobiome.org/). These primers (515F and 806R) carry unique barcodes that allow for multiplexed sequencing. Equimolar 16S rRNA PCR products from all samples were quantified and pooled prior to sequencing. Sequencing was performed by the Duke Sequencing and Genomic Technologies shared resource on an Illumina MiSeq instrument configured for 150 base-pair paired-end sequencing runs.

Subsequent data analysis was conducted in QIIME2 (https://qiime2.org), the successor of QIIME [101]. Paired reads were demultiplexed with qiime demux emp-paired, and denoised with qiime dada2 denoise-paired [102]. Taxonomy was assigned with qiime feature-classifier classify-sklearn [103], using a naive Bayes classifier, trained against the 99% clustered 16S reference sequence set of SILVA, v. 1.19 [104]. A basic statistical diversity analysis was performed, using qiime diversity core-metrics-phylogenetic, including alpha- and beta-diversity, as well as relative taxa abundances in sample groups. The determined relative taxa abundances were further analyzed with LEfSe (Linear discriminant analysis effect size) [105], to identify differential biomarkers in sample groups.

Statistical methods

All experiments were repeated at least two times and statistical analyses were performed with GraphPad Prism v.7. Data are presented as mean ± SEM. For comparisons between 2 groups a two tailed student's *t*-test or Mann-Whitney test was applied. For comparisons between 3 or more groups, a one-way ANOVA with Tukey's multiple comparisons test was used. For experiments with 2 independent variables, a two-way ANOVA was performed. Significance was set as $p < 0.05$, and denoted as: $^{*}\ p < 0.05$, $^{**}\ p < 0.01$, $^{***}\ p < 0.001$, $^{****}\ p < 0.0001$. Sample sizes are indicated in the figure legends.

Supporting information

S1 Fig. Generation of *saa* mutant zebrafish. (A) Sequence of CRISPR/Cas9 induced deletions in the coding region of zebrafish *saa* exon 2. **(B-C)** *In silico* translation of mutant allele *rdu60* revealed a frame shift mutation in exon 2 with a predicted early stop codon, indicated by the asterisk. **(D)** qRT-PCR of 6 dpf whole larvae demonstrated negligible *saa* mRNA expression in *saa* homozygous mutant zebrafish ($saa^{rdu60/rdu60}$ or $saa^{-/-}$). **(E)** qRT-PCR of 6 dpf whole larvae from trans-heterozygous $saa^{rdu60/rdu61}$ in-crosses revealed reduced *saa* mRNA levels relative to WT controls. **(F)** qRT-PCR of dissected digestive tracts from 6 dpf WT and $saa^{-/-}$ larvae demonstrated significantly reduced *saa* mRNA levels. **(G)** qRT-PCR of 6 dpf whole larvae from homozygous $saa^{rdu62/rdu62}$ in-crosses demonstrated reduced *saa* mRNA levels relative to WT controls. (qRT-PCR shown in panels D-G included 4–8 replicates / genotype, n ≥ 20 larvae / replicate). **(H)** Representative genotype distributions exhibited no deviation from expected Mendelian outcomes indicating no difference in viability of $saa^{-/-}$ animals ($p = 0.8257$) (from two independent experiments, actual number of animals from each genotype overlaid on bars). **(I-J)** Morphometric analysis illustrated loss of *saa* does not impact growth [standard length (SL), height at anterior of anal fin (HAA)] in 6 dpf larvae (n ≥ 26 larvae). **(K-L)** Confocal micrographs of transverse sections from transgenic WT and $saa^{-/-}$ 6 dpf larvae positive for $TgBAC(cldn15la{:}EGFP)^{pd1034Tg}$ (which labels IEC basolateral membranes with a Cldn15la-GFP fusion protein), and immunofluorescence labeling with the brush-border antibody 4E8 demonstrated intestinal architecture is qualitatively normal in mutant animals (scale bar = 50 μm).

(M) qRT-PCR of 6 dpf whole larvae following a tail amputation showed no significant induction of *saa*. **(N)** lyz:GFP^{+} neutrophil recruitment to caudal fin wound 6 hours following amputation in 6 dpf zebrafish larvae revealed decreased neutrophil recruitment in *saa* compound mutants (*saa*$^{rdu60/rdu62}$) versus WT controls (n $\geq$ 35 larvae / genotype at 6 hour time point). In panels D, F, G, I, J, M and N a *t*-test was used. In panel E, a Mann-Whitney test was applied. A chi-squared test was used to test for deviation from Mendelian distribution in H. Data are presented as mean ± SEM. * $p < 0.05$, ** $p < 0.01$, *** $p < 0.001$, **** $p < 0.0001$.
(TIF)

S2 Fig. Isolation and characterization of neutrophils from WT and *saa* mutant zebrafish larvae. (A) Gating strategy for isolation of lyz:EGFP^{+} neutrophils from 6 dpf zebrafish larvae. **(B)** The mean fluorescence intensity (MFI) of the lyz:EGFP^{+} neutrophil population was not significantly different between WT and *saa* mutant larvae. **(C)** qRT-PCR revealed no significant difference in *lysozyme C* (*lyz*) transcript levels in sorted lyz^{+} neutrophils from WT and *saa* mutant larvae. **(D)** Quantification of intracellular ROS levels as indicated by CellROX staining measured by flow cytometry in lyz:EGFP^{+} neutrophils from WT and *saa* mutant larvae showed no significant difference. **(E-F)** qRT-PCR analysis of sorted neutrophils revealed no differential expression of genes associated with pro-myelocyte progenitors (*cpa4*, *cpb1*, *cel.2*) or apoptotic markers (*cyba*, *p53*, *bcl2a*, *baxa*) between WT or *saa* mutants. (For panels B—F: n $\geq$ 4 replicates / genotype, n = 60–90 larvae / genotype). In panels B-F data was analyzed by *t*-test. Data are presented as mean ± SEM. * $p < 0.05$, ** $p < 0.01$, *** $p < 0.001$, **** $p < 0.0001$.
(TIF)

S3 Fig. Isolation and culture of zebrafish neutrophils *ex vivo*. (A) Gating strategy for isolation of CellROX labeled lyz:DsRed^{+} neutrophils from adult zebrafish kidneys. **(B-E)** Low magnification (10x) confocal images of lyz:EGFP^{+} neutrophils labeled with CellROX *ex vivo* (scale bar = 200 μm). **(F-G)** Imaging of CellROX labeled lyz:EGFP^{+} neutrophils isolated from WT and *saa* mutant zebrafish revealed cytoplasmic punctae (indicated by white arrows). Red dashed box indicates region enlarged to show cytoplasmic CellROX punctae (Scale bar = 20 μm). **(H)** The mean fluorescence intensity (MFI) of the lyz:DsRed^{+} population was unchanged between WT, *saa*$^{-/-}$, or *saa*$^{-/-}$;*Tg(cldn15la:saa)* neutrophils (4 replicates / genotype). **(I)** Quantification of intracellular ROS levels as indicated by CellROX staining measured by flow cytometry of lyz:DsRed^{+} neutrophils illustrated no significant difference in baseline CellROX levels between genotypes (4 replicates / genotype). **(J)** Measurement of lyz:EGFP^{+} neutrophil viability as assessed by Propidium Iodide (PI) staining demonstrated no significant differences between genotypes after 4 hours of co-culture with *E. coli* (relative to maximum PI signal from lysed neutrophils) (4 replicates / genotype). In panels H-I, data were analyzed by one-way ANOVA with Tukey's multiple comparisons test. In panel J, data were analyzed by *t*-test. Data are presented as mean ± SEM. * $p < 0.05$, ** $p < 0.01$, *** $p < 0.001$, **** $p < 0.0001$.
(TIF)

S4 Fig. Characterization of the zebrafish *cldn15la* promoter used to drive intestine-specific *saa* expression. (A) UCSC genome browser view of the zebrafish *cldn15la* gene locus with the translational start indicated by the red arrow. Pink bar represents the cloned 349 bp promoter region upstream of the *cldn15la* gene used to drive intestine-specific transgene expression. Tracks for vertebrate conservation, FAIRE-seq and motifs for transcription factors important of IEC gene expression programs (identified by HOMER) are shown below the locus [60]. **(B)** Expression pattern of endogenous *cldn15la* along the length of the intestine in adult zebrafish, as measured by microarray in Wang et al., 2010 [59]. **(C)** Representative stereoscope images of

IEC specific cytosolic mCherry expression in 5 dpf *Tg(-0.349cldn15la:mCherry)*^{rdu65} larvae compared to non-transgenic (NTG) controls (scale bar = 500 μm). White dashed line indicates the intestine. **(D)** Quantification of mCherry fluorescence in the indicated tissues of 6 dpf *Tg(-0.349cldn15la:mCherry)* and non-transgenic control larvae demonstrated intestine-restricted mCherry reporter activity (n = 7 larvae / genotype). **(E)** Representative confocal micrographs of immunostained transverse sections of *Tg(-0.349cldn15la:mCherry)* 6 dpf larvae along the anterior-posterior axis labeled with the absorptive cell brush border-specific antibody 4E8 illustrated transgene expression in absorptive enterocytes (scale bar = 20 μm). **(F)** Representative immunofluorescence images of transverse sections from *Tg(-0.349cldn15la:mCherry)* 6 dpf larvae stained with secretory cell-specific antibody 2F11 demonstrated weak expression in secretory cells, including enteroendocrine cells (outlined by red dashed lines) and goblet cells (outlined by green dashed lines) (scale bar = 20 μm). **(G)** Gating strategy for isolation of -0.349cldn15la:mCherry^{+} IECs from larval zebrafish. **(H)** qPCR for *mCherry* transcript in sorted *Tg(-0.349cldn15la:mCherry)* IECs showed enrichment as compared to negative fraction (13,000 –0.349cldn15la:mCherry^{+} or mCherry negative cells / replicate, 4 replicates / genotype, 30 larvae / replicate). Data in panel D analyzed by one-way ANOVA with Tukey's multiple comparison's test. Data in panel H analyzed by a Mann-Whitney test. Data are presented as mean ± SEM. * $p < 0.05$, ** $p < 0.01$, *** $p < 0.001$, **** $p < 0.0001$.
(TIF)

S5 Fig. Comparison of *Tg(-0.349cldn15la:mCherry)* and *TgBAC(cldn15la:EGFP)* expression patterns. (A) Widefield fluorescence images of IEC-specific cytosolic mCherry expression in 6 dpf double transgenic *Tg(-0.349cldn15la:mCherry)*^{rdu65}; *TgBAC(cldn15la:EGFP)*^{pd1034Tg} larvae demonstrated overlap in mCherry and GFP expression domains (scale bar = 500 μm). **(B)** Representative confocal micrographs of immunolabeled transverse sections from anterior (upper) and posterior (lower) intestinal segments of *Tg(-0.349cldn15la:mCherry)*^{rdu65};*TgBAC(cldn15la:EGFP)*^{pd1034Tg} 6 dpf larvae revealed expression of both mCherry and EGFP in IECs (scale bar = 20 μm). **(C)** Representative maximum intensity projections from single plane illumination microscopy (SPIM) z-stacks of *Tg(-0.349cldn15la:mCherry)*^{rdu65};*TgBAC(cldn15la:EGFP)* ^{pd1034Tg} 6 dpf larvae (scale bar = 500 μm). **(D-E)** High magnification single slice lightsheet images of the intestinal epithelium in a representative 6 dpf *Tg(-0.349cldn15la:mCherry)*^{rdu65};*TgBAC(cldn15la:EGFP)* ^{pd1034Tg} larva.
(TIF)

S6 Fig. Intestinal expression of zebrafish *saa* using *cldn15la* promoter. (A) qRT-PCR analysis of dissected digestive tracts and carcasses (remaining tissues following removal of the intestine) from 6 dpf larvae of indicated genotypes revealed significant increase in *saa* expression in transgenic larvae is restricted to the gut (4 replicates / genotype, 20 larvae / replicate). [73] **(B)** qRT-PCR of *saa* from whole 6 dpf larvae of the indicated genotypes (n = 4 replicates / genotype, 15–20 larvae / replicate). **(C)** Enumeration of lyz:DsRed^{+} wound-associated neutrophils at 6 hours post amputation revealed intestinally-derived saa does not affect neutrophil recruitment in WT larvae (n $\geq$ 32 larvae / genotype at 6 hour time point). **(D)** CFU quantification of bacterial concentration following 4 hour co-culture of lyz:DsRed^{+} adult zebrafish neutrophils with *E. coli* (MOI 2) (3–6 replicates / genotype). Data in panel A analyzed by a two-way ANOVA with *p* values reported in the table. Data in panel B was analyzed with a Kruskal-Wallis test. Data in panels C-D analyzed by one-way ANOVA with Tukey's multiple comparison's test. Data are presented as mean ± SEM. * $p < 0.05$, ** $p < 0.01$, *** $p < 0.001$, **** $p < 0.0001$.
(TIF)

S7 Fig. Transgenic Saa is insufficient to dampen transcriptional activation of neutrophils in *saa* mutant zebrafish larvae. (A) FACS revealed no significant difference in abundance of lyz:DsRed^{+} neutrophils in 6 dpf *saa*$^{-/-}$ larvae as compared to *saa*$^{-/-}$;*Tg(cldn15la:saa)* larvae (4 replicates / genotype / experiment, n $\geq$ 60 larvae / replicate, data pooled from 2 independent experiments). **(B)** qRT-PCR of pro-inflammatory mRNAs from lyz:DsRed^{+} neutrophils isolated from both *saa*$^{-/-}$ and *saa*$^{-/-}$;*Tg(cldn15la:saa)* larvae revealed persistent transcriptional activation as compared to WT (4 replicates / genotype, n $\geq$ 60 larvae / replicate). **(C)** FACS demonstrated increased abundance of lyz:DsRed^{+} neutrophils in 6 dpf *saa*$^{-/-}$ larvae which is restored to WT levels in *saa*$^{-/-}$;*Tg(fabp10a:saa)* larvae (4 replicates / genotype / experiment, n $\geq$ 60 larvae / replicate, data pooled from 2 independent experiments). **(D)** qRT-PCR of pro-inflammatory mRNAs from lyz:DsRed^{+} neutrophils isolated from both *saa*$^{-/-}$ and *saa*$^{-/-}$;*Tg(fabp10a:saa)* larvae revealed persistent transcriptional activation as compared to WT (4 replicates / genotype, n $\geq$ 60 larvae / replicate). Data in panels A-D were analyzed by one-way ANOVA with Tukey's multiple comparisons test. Data are presented as mean ± SEM. * $p < 0.05$, ** $p < 0.01$, *** $p < 0.001$, **** $p < 0.0001$.
(TIF)

S8 Fig. Neutrophil recruitment defects in *saa* deficient larvae are microbiota dependent. (A) lyz:EGFP^{+} neutrophil recruitment to caudal fin wound margin 6 hours after amputation in 6 dpf gnotobiotic GF WT and GF *saa*$^{-/-}$ zebrafish larvae was not significantly different (n $\geq$ 33 larvae / genotype / condition at the 6 hour timepoint). Data analyzed by a two-way ANOVA.
(TIF)

S1 Table. Primers used in this study (qRT-PCR, cloning and genotyping).
(PDF)

S2 Table. Statistical analysis of alpha-diversity comparisons from 16S rRNA gene sequencing (Kruskal-Wallis test). Bacterial communities in WT and *saa*$^{-/-}$ mutant (MUT) guts were not significantly different by any of these metrics, whereas WT/MUT guts were significantly different from their housing water (H2O) as expected.
(PDF)

S3 Table. Statistical analysis of beta-diversity comparisons from 16S rRNA gene sequencing (PERMANOVA). Bacterial communities in WT and *saa*$^{-/-}$ mutant (MUT) guts were not significantly different by any of these metrics, whereas WT/MUT guts were significantly different from their housing water (H2O) as expected.
(PDF)

Acknowledgments

The authors are grateful to Nancy Martin, and Bin Li, PhD and Mike Cook, PhD (Duke Cancer Institute Flow Cytometry Resource) for their assistance with FACS, and Lisa Cameron, PhD, Ben Carlson, PhD and Yasheng Gao, PhD (Duke Light Microscopy Core Facility) for their assistance with instrumentation. We are grateful to Holly Dressman, PhD and Zhengzheng Wei of the Duke Microbiome Shared Resource for DNA isolation and 16S rRNA gene sequencing. We are also grateful to Colin Lickwar, PhD for assistance and advice with bioinformatics. Finally, we are grateful to Jamie Garcia for assistance with Lightsheet microscopy.

Author Contributions

Conceptualization: Caitlin C. Murdoch, John F. Rawls.

Data curation: Olaf Mueller.

Formal analysis: Caitlin C. Murdoch, Scott T. Espenschied, Olaf Mueller.

Funding acquisition: Caitlin C. Murdoch, David M. Tobin, John F. Rawls.

Investigation: Caitlin C. Murdoch, Scott T. Espenschied, Molly A. Matty.

Methodology: Caitlin C. Murdoch, Scott T. Espenschied.

Resources: David M. Tobin.

Supervision: David M. Tobin, John F. Rawls.

Validation: Caitlin C. Murdoch.

Visualization: Caitlin C. Murdoch.

Writing – original draft: Caitlin C. Murdoch.

Writing – review & editing: Caitlin C. Murdoch, Scott T. Espenschied, Molly A. Matty, David M. Tobin, John F. Rawls.

References

1. Gensollen T, Iyer SS, Kasper DL, Blumberg RS. How colonization by microbiota in early life shapes the immune system. Science. 2016; 352(6285):539–44. https://doi.org/10.1126/science.aad9378 PMID: 27126036
2. Belkaid Y, Hand TW. Role of the microbiota in immunity and inflammation. Cell. 2014; 157(1):121–41. https://doi.org/10.1016/j.cell.2014.03.011 PMID: 24679531
3. Belkaid Y, Harrison OJ. Homeostatic Immunity and the Microbiota. Immunity. 2017; 46(4):562–76. https://doi.org/10.1016/j.immuni.2017.04.008 PMID: 28423337
4. Peterson LW, Artis D. Intestinal epithelial cells: regulators of barrier function and immune homeostasis. Nat Rev Immunol. 2014; 14(3):141–53. https://doi.org/10.1038/nri3608 PMID: 24566914
5. Wells JM, Brummer RJ, Derrien M, MacDonald TT, Troost F, Cani PD, et al. Homeostasis of the gut barrier and potential biomarkers. Am J Physiol Gastrointest Liver Physiol. 2017; 312(3):G171–G93. https://doi.org/10.1152/ajpgi.00048.2015 PMID: 27908847
6. Wells JM, Rossi O, Meijerink M, van Baarlen P. Epithelial crosstalk at the microbiota-mucosal interface. Proc Natl Acad Sci U S A. 2011; 108 Suppl 1:4607–14.
7. Davison JM, Lickwar CR, Song L, Breton G, Crawford GE, Rawls JF. Microbiota regulate intestinal epithelial gene expression by suppressing the transcription factor Hepatocyte nuclear factor 4 alpha. Genome Res. 2017; 27(7):1195–206. https://doi.org/10.1101/gr.220111.116 PMID: 28385711
8. Derebe MG, Zlatkov CM, Gattu S, Ruhn KA, Vaishnava S, Diehl GE, et al. Serum amyloid A is a retinol binding protein that transports retinol during bacterial infection. Elife. 2014; 3:e03206. https://doi.org/10.7554/eLife.03206 PMID: 25073702
9. El Aidy S, Merrifield CA, Derrien M, van Baarlen P, Hooiveld G, Levenez F, et al. The gut microbiota elicits a profound metabolic reorientation in the mouse jejunal mucosa during conventionalisation. Gut. 2013; 62(9):1306–14. https://doi.org/10.1136/gutjnl-2011-301955 PMID: 22722618
10. Kanther M, Sun X, Muhlbauer M, Mackey LC, Flynn EJ 3rd, Bagnat M, et al. Microbial colonization induces dynamic temporal and spatial patterns of NF-kappaB activation in the zebrafish digestive tract. Gastroenterology. 2011; 141(1):197–207. https://doi.org/10.1053/j.gastro.2011.03.042 PMID: 21439961
11. Rawls JF, Mahowald MA, Ley RE, Gordon JI. Reciprocal gut microbiota transplants from zebrafish and mice to germ-free recipients reveal host habitat selection. Cell. 2006; 127(2):423–33. https://doi.org/10.1016/j.cell.2006.08.043 PMID: 17055441
12. Kanther M, Tomkovich S, Xiaolun S, Grosser MR, Koo J, Flynn EJ 3rd, et al. Commensal microbiota stimulate systemic neutrophil migration through induction of serum amyloid A. Cell Microbiol. 2014; 16(7):1053–67. https://doi.org/10.1111/cmi.12257 PMID: 24373309
13. Uhlar CM, Whitehead AS. Serum amyloid A, the major vertebrate acute-phase reactant. Eur J Biochem. 1999; 265(2):501–23. PMID: 10504381

14. Gabay C, Kushner I. Acute-phase proteins and other systemic responses to inflammation. N Engl J Med. 1999; 340(6):448–54. https://doi.org/10.1056/NEJM199902113400607 PMID: 9971870

15. Steel DM, Whitehead AS. The major acute phase reactants: C-reactive protein, serum amyloid P component and serum amyloid A protein. Immunol Today. 1994; 15(2):81–8. https://doi.org/10.1016/0167-5699(94)90138-4 PMID: 8155266

16. Chambers RE, Stross P, Barry RE, Whicher JT. Serum amyloid A protein compared with C-reactive protein, alpha 1-antichymotrypsin and alpha 1-acid glycoprotein as a monitor of inflammatory bowel disease. Eur J Clin Invest. 1987; 17(5):460–7. PMID: 3121351

17. Noble CL, Abbas AR, Cornelius J, Lees CW, Ho GT, Toy K, et al. Regional variation in gene expression in the healthy colon is dysregulated in ulcerative colitis. Gut. 2008; 57(10):1398–405. https://doi.org/10.1136/gut.2008.148395 PMID: 18523026

18. Okahara S, Arimura Y, Yabana T, Kobayashi K, Gotoh A, Motoya S, et al. Inflammatory gene signature in ulcerative colitis with cDNA macroarray analysis. Aliment Pharmacol Ther. 2005; 21(9):1091–7. https://doi.org/10.1111/j.1365-2036.2005.02443.x PMID: 15854170

19. Scheja L, Heese B, Zitzer H, Michael MD, Siesky AM, Pospisil H, et al. Acute-phase serum amyloid A as a marker of insulin resistance in mice. Exp Diabetes Res. 2008; 2008:230837. https://doi.org/10.1155/2008/230837 PMID: 18584041

20. Yang RZ, Lee MJ, Hu H, Pollin TI, Ryan AS, Nicklas BJ, et al. Acute-phase serum amyloid A: an inflammatory adipokine and potential link between obesity and its metabolic complications. PLoS Med. 2006; 3(6):e287. https://doi.org/10.1371/journal.pmed.0030287 PMID: 16737350

21. Badolato R, Wang JM, Murphy WJ, Lloyd AR, Michiel DF, Bausserman LL, et al. Serum amyloid A is a chemoattractant: induction of migration, adhesion, and tissue infiltration of monocytes and polymorphonuclear leukocytes. J Exp Med. 1994; 180(1):203–9. PMID: 7516407

22. Cai H, Song C, Endoh I, Goyette J, Jessup W, Freedman SB, et al. Serum amyloid A induces monocyte tissue factor. J Immunol. 2007; 178(3):1852–60. PMID: 17237436

23. Furlaneto CJ, Campa A. A novel function of serum amyloid A: a potent stimulus for the release of tumor necrosis factor-alpha, interleukin-1beta, and interleukin-8 by human blood neutrophil. Biochem Biophys Res Commun. 2000; 268(2):405–8. https://doi.org/10.1006/bbrc.2000.2143 PMID: 10679217

24. He R, Sang H, Ye RD. Serum amyloid A induces IL-8 secretion through a G protein-coupled receptor, FPRL1/LXA4R. Blood. 2003; 101(4):1572–81. https://doi.org/10.1182/blood-2002-05-1431 PMID: 12393391

25. Patel H, Fellowes R, Coade S, Woo P. Human serum amyloid A has cytokine-like properties. Scand J Immunol. 1998; 48(4):410–8. PMID: 9790312

26. Atarashi K, Tanoue T, Ando M, Kamada N, Nagano Y, Narushima S, et al. Th17 Cell Induction by Adhesion of Microbes to Intestinal Epithelial Cells. Cell. 2015; 163(2):367–80. https://doi.org/10.1016/j.cell.2015.08.058 PMID: 26411289

27. Sano T, Huang W, Hall JA, Yang Y, Chen A, Gavzy SJ, et al. An IL-23R/IL-22 Circuit Regulates Epithelial Serum Amyloid A to Promote Local Effector Th17 Responses. Cell. 2015; 163(2):381–93. https://doi.org/10.1016/j.cell.2015.08.061 PMID: 26411290

28. Christenson K, Bjorkman L, Ahlin S, Olsson M, Sjoholm K, Karlsson A, et al. Endogenous Acute Phase Serum Amyloid A Lacks Pro-Inflammatory Activity, Contrasting the Two Recombinant Variants That Activate Human Neutrophils through Different Receptors. Front Immunol. 2013; 4:92. https://doi.org/10.3389/fimmu.2013.00092 PMID: 23626589

29. Kim MH, de Beer MC, Wroblewski JM, Webb NR, de Beer FC. SAA does not induce cytokine production in physiological conditions. Cytokine. 2013; 61(2):506–12. https://doi.org/10.1016/j.cyto.2012.10.019 PMID: 23165195

30. Deniset JF, Kubes P. Recent advances in understanding neutrophils. F1000Res. 2016; 5:2912. https://doi.org/10.12688/f1000research.9691.1 PMID: 28105328

31. Kolaczkowska E, Kubes P. Neutrophil recruitment and function in health and inflammation. Nat Rev Immunol. 2013; 13(3):159–75. https://doi.org/10.1038/nri3399 PMID: 23435331

32. El-Benna J, Hurtado-Nedelec M, Marzaioli V, Marie JC, Gougerot-Pocidalo MA, Dang PM. Priming of the neutrophil respiratory burst: role in host defense and inflammation. Immunol Rev. 2016; 273(1):180–93. https://doi.org/10.1111/imr.12447 PMID: 27558335

33. Miralda I, Uriarte SM, McLeish KR. Multiple Phenotypic Changes Define Neutrophil Priming. Front Cell Infect Microbiol. 2017; 7:217. https://doi.org/10.3389/fcimb.2017.00217 PMID: 28611952

34. Balmer ML, Schurch CM, Saito Y, Geuking MB, Li H, Cuenca M, et al. Microbiota-derived compounds drive steady-state granulopoiesis via MyD88/TICAM signaling. J Immunol. 2014; 193(10):5273–83. https://doi.org/10.4049/jimmunol.1400762 PMID: 25305320

35. Bugl S, Wirths S, Radsak MP, Schild H, Stein P, Andre MC, et al. Steady-state neutrophil homeostasis is dependent on TLR4/TRIF signaling. Blood. 2013; 121(5):723–33. https://doi.org/10.1182/blood-2012-05-429589 PMID: 23223360

36. Clarke TB, Davis KM, Lysenko ES, Zhou AY, Yu Y, Weiser JN. Recognition of peptidoglycan from the microbiota by Nod1 enhances systemic innate immunity. Nat Med. 2010; 16(2):228–31. https://doi.org/10.1038/nm.2087 PMID: 20081863

37. Deshmukh HS, Liu Y, Menkiti OR, Mei J, Dai N, O'Leary CE, et al. The microbiota regulates neutrophil homeostasis and host resistance to Escherichia coli K1 sepsis in neonatal mice. Nat Med. 2014; 20 (5):524–30. https://doi.org/10.1038/nm.3542 PMID: 24747744

38. Karmarkar D, Rock KL. Microbiota signalling through MyD88 is necessary for a systemic neutrophilic inflammatory response. Immunology. 2013; 140(4):483–92. https://doi.org/10.1111/imm.12159 PMID: 23909393

39. Zhang D, Chen G, Manwani D, Mortha A, Xu C, Faith JJ, et al. Neutrophil ageing is regulated by the microbiome. Nature. 2015; 525(7570):528–32. https://doi.org/10.1038/nature15367 PMID: 26374999

40. Hall C, Flores MV, Storm T, Crosier K, Crosier P. The zebrafish lysozyme C promoter drives myeloid-specific expression in transgenic fish. BMC Dev Biol. 2007; 7:42. https://doi.org/10.1186/1471-213X-7-42 PMID: 17477879

41. Harvie EA, Huttenlocher A. Neutrophils in host defense: new insights from zebrafish. J Leukoc Biol. 2015; 98(4):523–37. https://doi.org/10.1189/jlb.4MR1114-524R PMID: 25717145

42. Keightley MC, Carradice DP, Layton JE, Pase L, Bertrand JY, Wittig JG, et al. The Pu.1 target gene Zbtb11 regulates neutrophil development through its integrase-like HHCC zinc finger. Nat Commun. 2017; 8:14911. https://doi.org/10.1038/ncomms14911 PMID: 28382966

43. Malcolm KC, Arndt PG, Manos EJ, Jones DA, Worthen GS. Microarray analysis of lipopolysaccharide-treated human neutrophils. Am J Physiol Lung Cell Mol Physiol. 2003; 284(4):L663–70. https://doi.org/10.1152/ajplung.00094.2002 PMID: 12495940

44. Subrahmanyam YV, Yamaga S, Prashar Y, Lee HH, Hoe NP, Kluger Y, et al. RNA expression patterns change dramatically in human neutrophils exposed to bacteria. Blood. 2001; 97(8):2457–68. PMID: 11290611

45. Wright HL, Thomas HB, Moots RJ, Edwards SW. RNA-seq reveals activation of both common and cytokine-specific pathways following neutrophil priming. PLoS One. 2013; 8(3):e58598. https://doi.org/10.1371/journal.pone.0058598 PMID: 23554905

46. Yao Y, Matsushima H, Ohtola JA, Geng S, Lu R, Takashima A. Neutrophil priming occurs in a sequential manner and can be visualized in living animals by monitoring IL-1beta promoter activation. J Immunol. 2015; 194(3):1211–24. https://doi.org/10.4049/jimmunol.1402018 PMID: 25527787

47. Zhang X, Kluger Y, Nakayama Y, Poddar R, Whitney C, DeTora A, et al. Gene expression in mature neutrophils: early responses to inflammatory stimuli. J Leukoc Biol. 2004; 75(2):358–72. https://doi.org/10.1189/jlb.0903412 PMID: 14634056

48. Borregaard N. Neutrophils, from marrow to microbes. Immunity. 2010; 33(5):657–70. https://doi.org/10.1016/j.immuni.2010.11.011 PMID: 21094463

49. Mayadas TN, Cullere X, Lowell CA. The multifaceted functions of neutrophils. Annu Rev Pathol. 2014; 9:181–218. https://doi.org/10.1146/annurev-pathol-020712-164023 PMID: 24050624

50. Urieli-Shoval S, Linke RP, Matzner Y. Expression and function of serum amyloid A, a major acute-phase protein, in normal and disease states. Curr Opin Hematol. 2000; 7(1):64–9. PMID: 10608507

51. Cheung ID, Bagnat M, Ma TP, Datta A, Evason K, Moore JC, et al. Regulation of intrahepatic biliary duct morphogenesis by Claudin 15-like b. Dev Biol. 2012; 361(1):68–78. https://doi.org/10.1016/j.ydbio.2011.10.004 PMID: 22020048

52. Cox AG, Hwang KL, Brown KK, Evason K, Beltz S, Tsomides A, et al. Yap reprograms glutamine metabolism to increase nucleotide biosynthesis and enable liver growth. Nat Cell Biol. 2016; 18 (8):886–96. https://doi.org/10.1038/ncb3389 PMID: 27428308

53. Cox AG, Saunders DC, Kelsey PB Jr., Conway AA, Tesmenitsky Y, Marchini JF, et al. S-nitrosothiol signaling regulates liver development and improves outcome following toxic liver injury. Cell Rep. 2014; 6(1):56–69. https://doi.org/10.1016/j.celrep.2013.12.007 PMID: 24388745

54. Her GM, Chiang CC, Chen WY, Wu JL. In vivo studies of liver-type fatty acid binding protein (L-FABP) gene expression in liver of transgenic zebrafish (Danio rerio). FEBS Lett. 2003; 538(1–3):125–33. PMID: 12633865

55. Clatworthy AE, Lee JS, Leibman M, Kostun Z, Davidson AJ, Hung DT. Pseudomonas aeruginosa infection of zebrafish involves both host and pathogen determinants. Infect Immun. 2009; 77(4):1293–303. https://doi.org/10.1128/IAI.01181-08 PMID: 19168742

56. Herbomel P, Thisse B, Thisse C. Ontogeny and behaviour of early macrophages in the zebrafish embryo. Development. 1999; 126(17):3735–45. PMID: 10433904

57. Her GM, Chiang CC, Wu JL. Zebrafish intestinal fatty acid binding protein (I-FABP) gene promoter drives gut-specific expression in stable transgenic fish. Genesis. 2004; 38(1):26–31. https://doi.org/10.1002/gene.10248 PMID: 14755801

58. Alvers AL, Ryan S, Scherz PJ, Huisken J, Bagnat M. Single continuous lumen formation in the zebrafish gut is mediated by smoothened-dependent tissue remodeling. Development. 2014; 141(5):1110–9. https://doi.org/10.1242/dev.100313 PMID: 24504339

59. Wang Z, Du J, Lam SH, Mathavan S, Matsudaira P, Gong Z. Morphological and molecular evidence for functional organization along the rostrocaudal axis of the adult zebrafish intestine. BMC Genomics. 2010; 11:392. https://doi.org/10.1186/1471-2164-11-392 PMID: 20565988

60. Lickwar CR, Camp JG, Weiser M, Cocchiaro JL, Kingsley DM, Furey TS, et al. Genomic dissection of conserved transcriptional regulation in intestinal epithelial cells. PLoS Biol. 2017; 15(8):e2002054. https://doi.org/10.1371/journal.pbio.2002054 PMID: 28850571

61. Flores MV, Hall CJ, Davidson AJ, Singh PP, Mahagaonkar AA, Zon LI, et al. Intestinal differentiation in zebrafish requires Cdx1b, a functional equivalent of mammalian Cdx2. Gastroenterology. 2008; 135 (5):1665–75. https://doi.org/10.1053/j.gastro.2008.07.024 PMID: 18804112

62. Brannon MK, Davis JM, Mathias JR, Hall CJ, Emerson JC, Crosier PS, et al. Pseudomonas aeruginosa Type III secretion system interacts with phagocytes to modulate systemic infection of zebrafish embryos. Cell Microbiol. 2009; 11(5):755–68. https://doi.org/10.1111/j.1462-5822.2009.01288.x PMID: 19207728

63. Phennicie RT, Sullivan MJ, Singer JT, Yoder JA, Kim CH. Specific resistance to Pseudomonas aeruginosa infection in zebrafish is mediated by the cystic fibrosis transmembrane conductance regulator. Infect Immun. 2010; 78(11):4542–50. https://doi.org/10.1128/IAI.00302-10 PMID: 20732993

64. Eckhardt ER, Witta J, Zhong J, Arsenescu R, Arsenescu V, Wang Y, et al. Intestinal epithelial serum amyloid A modulates bacterial growth in vitro and pro-inflammatory responses in mouse experimental colitis. BMC Gastroenterol. 2010; 10:133. https://doi.org/10.1186/1471-230X-10-133 PMID: 21067563

65. Hari-Dass R, Shah C, Meyer DJ, Raynes JG. Serum amyloid A protein binds to outer membrane protein A of gram-negative bacteria. J Biol Chem. 2005; 280(19):18562–7. https://doi.org/10.1074/jbc.M500490200 PMID: 15705572

66. Hirakura Y, Carreras I, Sipe JD, Kagan BL. Channel formation by serum amyloid A: a potential mechanism for amyloid pathogenesis and host defense. Amyloid. 2002; 9(1):13–23. PMID: 12000193

67. Hergott CB, Roche AM, Tamashiro E, Clarke TB, Bailey AG, Laughlin A, et al. Peptidoglycan from the gut microbiota governs the lifespan of circulating phagocytes at homeostasis. Blood. 2016; 127 (20):2460–71. https://doi.org/10.1182/blood-2015-10-675173 PMID: 26989200

68. Hatanaka E, Furlaneto CJ, Ribeiro FP, Souza GM, Campa A. Serum amyloid A-induced mRNA expression and release of tumor necrosis factor-alpha (TNF-alpha) in human neutrophils. Immunol Lett. 2004; 91(1):33–7. PMID: 14757367

69. Hatanaka E, Monteagudo PT, Marrocos MS, Campa A. Interaction between serum amyloid A and leukocytes—a possible role in the progression of vascular complications in diabetes. Immunol Lett. 2007; 108(2):160–6. https://doi.org/10.1016/j.imlet.2006.12.005 PMID: 17267050

70. Hatanaka E, Pereira Ribeiro F, Campa A. The acute phase protein serum amyloid A primes neutrophils. FEMS Immunol Med Microbiol. 2003; 38(1):81–4. https://doi.org/10.1016/S0928-8244(03)00112-3 PMID: 12900059

71. Migita K, Izumi Y, Jiuchi Y, Kozuru H, Kawahara C, Nakamura M, et al. Serum amyloid A induces NLRP-3-mediated IL-1beta secretion in neutrophils. PLoS One. 2014; 9(5):e96703. https://doi.org/10.1371/journal.pone.0096703 PMID: 24846290

72. Ribeiro FP, Furlaneto CJ, Hatanaka E, Ribeiro WB, Souza GM, Cassatella MA, et al. mRNA expression and release of interleukin-8 induced by serum amyloid A in neutrophils and monocytes. Mediators Inflamm. 2003; 12(3):173–8. https://doi.org/10.1080/0962935031000134897 PMID: 12857601

73. Bates JM, Akerlund J, Mittge E, Guillemin K. Intestinal alkaline phosphatase detoxifies lipopolysaccharide and prevents inflammation in zebrafish in response to the gut microbiota. Cell Host Microbe. 2007; 2(6):371–82. https://doi.org/10.1016/j.chom.2007.10.010 PMID: 18078689

74. Galindo-Villegas J, Garcia-Moreno D, de Oliveira S, Meseguer J, Mulero V. Regulation of immunity and disease resistance by commensal microbes and chromatin modifications during zebrafish development. Proc Natl Acad Sci U S A. 2012; 109(39):E2605–14. https://doi.org/10.1073/pnas.1209920109 PMID: 22949679

75. Cox LM, Yamanishi S, Sohn J, Alekseyenko AV, Leung JM, Cho I, et al. Altering the intestinal microbiota during a critical developmental window has lasting metabolic consequences. Cell. 2014; 158 (4):705–21. https://doi.org/10.1016/j.cell.2014.05.052 PMID: 25126780

76. Ekmekciu I, von Klitzing E, Fiebiger U, Escher U, Neumann C, Bacher P, et al. Immune Responses to Broad-Spectrum Antibiotic Treatment and Fecal Microbiota Transplantation in Mice. Front Immunol. 2017; 8:397. https://doi.org/10.3389/fimmu.2017.00397 PMID: 28469619

77. Sekirov I, Tam NM, Jogova M, Robertson ML, Li Y, Lupp C, et al. Antibiotic-induced perturbations of the intestinal microbiota alter host susceptibility to enteric infection. Infect Immun. 2008; 76(10):4726–36. https://doi.org/10.1128/IAI.00319-08 PMID: 18678663

78. Morgun A, Dzutsev A, Dong X, Greer RL, Sexton DJ, Ravel J, et al. Uncovering effects of antibiotics on the host and microbiota using transkingdom gene networks. Gut. 2015; 64(11):1732–43. https://doi.org/10.1136/gutjnl-2014-308820 PMID: 25614621

79. Yoon MY, Yoon SS. Disruption of the Gut Ecosystem by Antibiotics. Yonsei Med J. 2018; 59(1):4–12. https://doi.org/10.3349/ymj.2018.59.1.4 PMID: 29214770

80. Coetzee GA, Strachan AF, van der Westhuyzen DR, Hoppe HC, Jeenah MS, de Beer FC. Serum amyloid A-containing human high density lipoprotein 3. Density, size, and apolipoprotein composition. J Biol Chem. 1986; 261(21):9644–51. PMID: 3525531

81. Camp JG, Frank CL, Lickwar CR, Guturu H, Rube T, Wenger AM, et al. Microbiota modulate transcription in the intestinal epithelium without remodeling the accessible chromatin landscape. Genome Res. 2014; 24(9):1504–16. https://doi.org/10.1101/gr.165845.113 PMID: 24963153

82. Gutfeld O, Prus D, Ackerman Z, Dishon S, Linke RP, Levin M, et al. Expression of serum amyloid A, in normal, dysplastic, and neoplastic human colonic mucosa: implication for a role in colonic tumorigenesis. J Histochem Cytochem. 2006; 54(1):63–73. https://doi.org/10.1369/jhc.5A6645.2005 PMID: 16116035

83. Reigstad CS, Backhed F. Microbial regulation of SAA3 expression in mouse colon and adipose tissue. Gut Microbes. 2010; 1(1):55–7. https://doi.org/10.4161/gmic.1.1.10514 PMID: 21327118

84. Larsson E, Tremaroli V, Lee YS, Koren O, Nookaew I, Fricker A, et al. Analysis of gut microbial regulation of host gene expression along the length of the gut and regulation of gut microbial ecology through MyD88. Gut. 2012; 61(8):1124–31. https://doi.org/10.1136/gutjnl-2011-301104 PMID: 22115825

85. Zhang G, Liu J, Wu L, Fan Y, Sun L, Qian F, et al. Elevated Expression of Serum Amyloid A 3 Protects Colon Epithelium Against Acute Injury Through TLR2-Dependent Induction of Neutrophil IL-22 Expression in a Mouse Model of Colitis. Front Immunol. 2018; 9:1503. https://doi.org/10.3389/fimmu.2018.01503 PMID: 30008720

86. Ivanov II, Atarashi K, Manel N, Brodie EL, Shima T, Karaoz U, et al. Induction of intestinal Th17 cells by segmented filamentous bacteria. Cell. 2009; 139(3):485–98. https://doi.org/10.1016/j.cell.2009.09.033 PMID: 19836068

87. Rawls JF, Mahowald MA, Goodman AL, Trent CM, Gordon JI. In vivo imaging and genetic analysis link bacterial motility and symbiosis in the zebrafish gut. Proc Natl Acad Sci U S A. 2007; 104 (18):7622–7. https://doi.org/10.1073/pnas.0702386104 PMID: 17456593

88. Frame NM, Gursky O. Structure of serum amyloid A suggests a mechanism for selective lipoprotein binding and functions: SAA as a hub in macromolecular interaction networks. FEBS Lett. 2016; 590 (6):866–79. https://doi.org/10.1002/1873-3468.12116 PMID: 26918388

89. Summers C, Rankin SM, Condliffe AM, Singh N, Peters AM, Chilvers ER. Neutrophil kinetics in health and disease. Trends Immunol. 2010; 31(8):318–24. https://doi.org/10.1016/j.it.2010.05.006 PMID: 20620114

90. Kenyon A, Gavriouchkina D, Zorman J, Napolitani G, Cerundolo V, Sauka-Spengler T. Active nuclear transcriptome analysis reveals inflammasome-dependent mechanism for early neutrophil response to Mycobacterium marinum. Sci Rep. 2017; 7(1):6505. https://doi.org/10.1038/s41598-017-06099-x PMID: 28747644

91. Kobayashi SD, Voyich JM, Braughton KR, Whitney AR, Nauseef WM, Malech HL, et al. Gene expression profiling provides insight into the pathophysiology of chronic granulomatous disease. J Immunol. 2004; 172(1):636–43. PMID: 14688376

92. Kruger P, Saffarzadeh M, Weber AN, Rieber N, Radsak M, von Bernuth H, et al. Neutrophils: Between host defence, immune modulation, and tissue injury. PLoS Pathog. 2015; 11(3):e1004651. https://doi.org/10.1371/journal.ppat.1004651 PMID: 25764063

93. Segel GB, Halterman MW, Lichtman MA. The paradox of the neutrophil's role in tissue injury. J Leukoc Biol. 2011; 89(3):359–72. https://doi.org/10.1189/jlb.0910538 PMID: 21097697

94. Wang J. Neutrophils in tissue injury and repair. Cell Tissue Res. 2018; 371(3):531–9. https://doi.org/10.1007/s00441-017-2785-7 PMID: 29383445

95. Ather JL, Poynter ME. Serum amyloid A3 is required for normal weight and immunometabolic function in mice. PLoS One. 2018; 13(2):e0192352. https://doi.org/10.1371/journal.pone.0192352 PMID: 29390039

96. Ye RD, Sun L. Emerging functions of serum amyloid A in inflammation. J Leukoc Biol. 2015; 98 (6):923–9. https://doi.org/10.1189/jlb.3VMR0315-080R PMID: 26130702

97. Evrard M, Kwok IWH, Chong SZ, Teng KWW, Becht E, Chen J, et al. Developmental Analysis of Bone Marrow Neutrophils Reveals Populations Specialized in Expansion, Trafficking, and Effector Functions. Immunity. 2018; 48(2):364–79 e8. https://doi.org/10.1016/j.immuni.2018.02.002 PMID: 29466759

98. Pham LN, Kanther M, Semova I, Rawls JF. Methods for generating and colonizing gnotobiotic zebrafish. Nat Protoc. 2008; 3(12):1862–75. https://doi.org/10.1038/nprot.2008.186 PMID: 19008873

99. Jao LE, Wente SR, Chen W. Efficient multiplex biallelic zebrafish genome editing using a CRISPR nuclease system. Proc Natl Acad Sci U S A. 2013; 110(34):13904–9. https://doi.org/10.1073/pnas.1308335110 PMID: 23918387

100. Beerman RW, Matty MA, Au GG, Looger LL, Choudhury KR, Keller PJ, et al. Direct In Vivo Manipulation and Imaging of Calcium Transients in Neutrophils Identify a Critical Role for Leading-Edge Calcium Flux. Cell Rep. 2015; 13(10):2107–17. https://doi.org/10.1016/j.celrep.2015.11.010 PMID: 26673320

101. Caporaso JG, Kuczynski J, Stombaugh J, Bittinger K, Bushman FD, Costello EK, et al. QIIME allows analysis of high-throughput community sequencing data. Nat Methods. 2010; 7(5):335–6. https://doi.org/10.1038/nmeth.f.303 PMID: 20383131

102. Callahan BJ, McMurdie PJ, Rosen MJ, Han AW, Johnson AJ, Holmes SP. DADA2: High-resolution sample inference from Illumina amplicon data. Nat Methods. 2016; 13(7):581–3. https://doi.org/10.1038/nmeth.3869 PMID: 27214047

103. Fabian Pedregosa GV, Alexandre Gramfort, Vincent Michel, Bertrand Thirion, Olivier Grisel, Mathieu Blondel, Andreas Müller, Joel Nothman, Gilles Louppe, Peter Prettenhofer, Ron Weiss, Vincent Dubourg, Jake Vanderplas, Alexandre Passos, David Cournapeau, Matthieu Brucher, Matthieu Perrot, Édouard Duchesnay. Scikit-learn: Machine Learning in Python. Journal of Machine Learning Research. 2011; 12:2825–30.

104. Quast C, Pruesse E, Yilmaz P, Gerken J, Schweer T, Yarza P, et al. The SILVA ribosomal RNA gene database project: improved data processing and web-based tools. Nucleic Acids Res. 2013; 41(Database issue):D590–6. https://doi.org/10.1093/nar/gks1219 PMID: 23193283

105. Segata N, Izard J, Waldron L, Gevers D, Miropolsky L, Garrett WS, et al. Metagenomic biomarker discovery and explanation. Genome Biol. 2011; 12(6):R60. https://doi.org/10.1186/gb-2011-12-6-r60 PMID: 21702898